Phage-induced efflux down-regulation boosts antibiotic efficacy

Samuel Kraus[1], Urszula Łapińska[1], Krina Chawla[1], Evan Baker[2,3], Erin L Attrill[1], Paul O'Neill[4], Audrey Farbos[4], Aaron Jeffries[4], Edouard E. Galyov[5], Sunee Korbsrisate[6], Kay B. Barnes[7], Sarah V Harding[7], Krasimira Tsaneva-Atanasova[2,3], Mark A T Blaskovich[8], Stefano Pagliara[1,9*]

[1]Living Systems Institute and Biosciences, University of Exeter, Exeter, Devon, EX4 4QD, United Kingdom
[2]Department of Mathematics and Living Systems Institute, University of Exeter, Exeter, Devon, EX4 4QD, United Kingdom
[3]EPSRC Hub for Quantitative Modelling in Healthcare, University of Exeter, Exeter, EX4 4QJ, UK
[4]Biosciences, University of Exeter, Exeter, Devon, EX4 4QD, United Kingdom
[5]Department of Genetics and Genome Biology, University of Leicester, University Road, Leicester, LE1 7RH, United Kingdom
[6]Department of Immunology, Faculty of Medicine Siriraj Hospital, Mahidol University, Bangkok 10700, Thailand
[7]Defence Science and Technology Laboratory, Porton Down, Salisbury, Wiltshire, SP4 0JQ, United Kingdom
[8]Centre for Superbug Solutions, Institute for Molecular Bioscience, The University of Queensland, St. Lucia, QLD, 4072, Australia
[9]Lead contact
*Correspondence: s.pagliara@exeter.ac.uk

Summary

The interactions between a virus and its host vary in space and time and are affected by the presence of molecules that alter the physiology of either the host or the virus. Determining the molecular mechanisms underpinning these interactions is paramount for predicting the fate of bacterial and phage populations and for designing rational phage-antibiotic therapies. We study the interactions between stationary phase *Burkholderia thailandensis* and the phage ΦBp-AMP1. Although heterogeneous genetic resistance to phage rapidly emerges in *B. thailandensis*, the presence of phage enhances the efficacy of three major antibiotic classes, the quinolones, the beta-lactams and the tetracyclines, but antagonizes tetrahydrofolate synthesis inhibitors. We discovered that enhanced antibiotic efficacy is underpinned by reduced antibiotic efflux in the presence of phage. This new phage-antibiotic therapy allows for eradication of stationary phase bacteria, whilst requiring reduced antibiotic concentrations, which is crucial for treating infections in sites where it is difficult to achieve high antibiotic concentrations.

Keywords

Antimicrobial resistance; phage-antibiotic therapy; *Burkholderia thailandensis*; bacteriophage resistance; membrane transport; efflux; transcriptomics; gene expression; antibiotics; antibiotic accumulation

Introduction

Antimicrobial resistance (AMR) has a dramatic impact on global health with an estimated 5 million deaths associated with AMR in 2019 alone [1]. *Burkholderia* Bptm species cause life-threatening diseases [2–5] and are challenging to treat with currently available antibiotics as they are intrinsically resistant to aminoglycosides, macrolides and oxazolidinones due to constitutively expressed efflux pumps [6–9], whereas an atypical lipopolysaccharide structure plays a crucial role in resistance to cationic peptides such as polymyxins [2].

Moreover, misuse and overuse of antibiotics in the food industry, animal husbandry, and medicine, as well as changes in the global environment have recently contributed to the spread of acquired genetic resistance [10]. *Burkholderia* Bptm species can acquire antibiotic resistance *in vivo* during treatment, which can be fatal if treatment is not shifted to alternative drugs in due course [2].

In order to overcome the development of resistance to antibiotic monotherapies, the deployment of two or more different antibiotics in combination therapies has shown some success in treating and preventing infections [11,12]; however, antibiotics in conventional regimens can antagonize each other [13,14]. Therefore, several alternatives to traditional antibiotics have been explored in order to treat resistant infections, including: antibody therapy, antimicrobial peptides, probiotics, metal chelation, CRISPR-Cas9, bioengineered toxins, bacteriocins, vaccines and antibodies [15–19]. Although promising, all of these approaches are limited by the fact that these antimicrobial agents cannot change or adapt in real time.

In contrast, like bacteria, bacteriophages (i.e., viruses that infect bacteria) amplify at the site of an infection and evolve; therefore, also due to their high number and genetic variability, phage constitute a large and valuable reservoir of natural antimicrobials [20]. However, the use of phage as a monotherapy to treat bacterial infections presents several challenges, particularly narrow host range and the rapid evolution of resistance to phage [21]. As antibiotics are the current standard of care, using phage as an adjuvant to antibiotics instead of a monotherapy may be a more rational therapeutic use of phage [22]. Therefore, phage-antibiotic therapy has undergone a robust revitalization in the last seven years [23–25].

Enchanced efficacy of combination therapies has historically been attributed to an increase in phage produced from bacteria in the presence of β-lactam antibiotics, relative to production in their absence [26,27]. More recently, a variety of lytic phage was observed to form larger plaques in the presence of sublethal concentrations of β-lactam, quinolone and tetracycline antibiotics [28–31]. This effect has been termed phage-antibiotic synergy and has been linked to antibiotic-induced bacterial filamentation which accelerates phage assembly and cell lysis [28]. However,

77 other recent evidence suggests that phage-antibiotic synergy can be obtained independently
78 of cell filamentation, enhancement of phage production or the strict use of lytic phage, and
79 that temperate phage are also viable for phage-antibiotic therapy if prophages are induced by
80 DNA damaging antibiotics [32].

81 Moreover, phage-antibiotic synergy has mostly been studied with only one or two
82 concentrations of the antimicrobials, which is insufficient to predict combinatorial
83 concentrations that are effective during treatment, leading to mixed results during phage-
84 antibiotic therapy investigations [22,33]. Indeed, a recent study employing *Escherichia coli* and
85 the lytic phage ϕHP3 tested several orders of magnitude of both phage and antibiotic
86 concentrations, finding that the nature of the interaction between antibiotics and phage
87 depended both on the type and concentration of the antibiotic and phage employed [34].

88 Therefore, it is imperative to discover and understand the molecular mechanisms
89 underpinning the interactions between phage and antibiotics, in order to rationally design
90 successful new phage-antibiotic therapy [20]. Here we test molecules representative of eight
91 major antibiotic classes in combination with a recently discovered phage, termed ΦBp-AMP1,
92 that infects and kills *Burkholderia pseudomallei* and *Burkholderia thailandensis* [35–37]. ΦBp-
93 AMP1 is a podovirus with a 45 nm icosahedral capsid, a 20 nm non-contractile tail and a 45
94 kb genome. In contrast to other *Burkholderia* phage that are strictly lytic [38], ΦBp-AMP1
95 displays a temperature-dependent switch from the temperate (at 25 °C) to the lytic cycle (at
96 37 °C) [35–37]. Using optically based microtiter plate assays and genomics, we studied the
97 development of genetic resistance to ΦBp-AMP1 in stationary phase *B. thailandensis*. We
98 investigated the dynamics of the interactions between ΦBp-AMP1 and representative
99 molecules of the major antibiotic classes over multiple orders of magnitude of antibiotic
100 concentrations and phage titers. We determined the molecular mechanisms underpinning
101 these phage-antibiotic interactions via single-cell microscopy, mathematical modelling and
102 gene expression profiling of stationary phase *B. thailandensis* undergoing phage-antibiotic
103 combination therapy as well as antibiotic or phage monotherapy.

104

105 **Results**

106 **Genetic resistance to ΦBp-AMP1 phage in *B. thailandensis* is heterogeneous**

107 We used well-mixed liquid cultures of stationary phase *B. thailandensis* (strain E264) with
108 ΦBp-AMP1 at a multiplicity of infection (MOI) of 1 in lysogeny broth (LB) medium at 37 °C and
109 performed colony forming unit (CFU) assays every 2 h over a 24 h period. For the first 14 h of
110 incubation in the presence of phage, we did not observe neither a reduction nor an increase

of the bacterial population, despite the presence of LB medium allowed regrowth of uninfected stationary phase *B. thailandensis* cultures (Figure 1A).

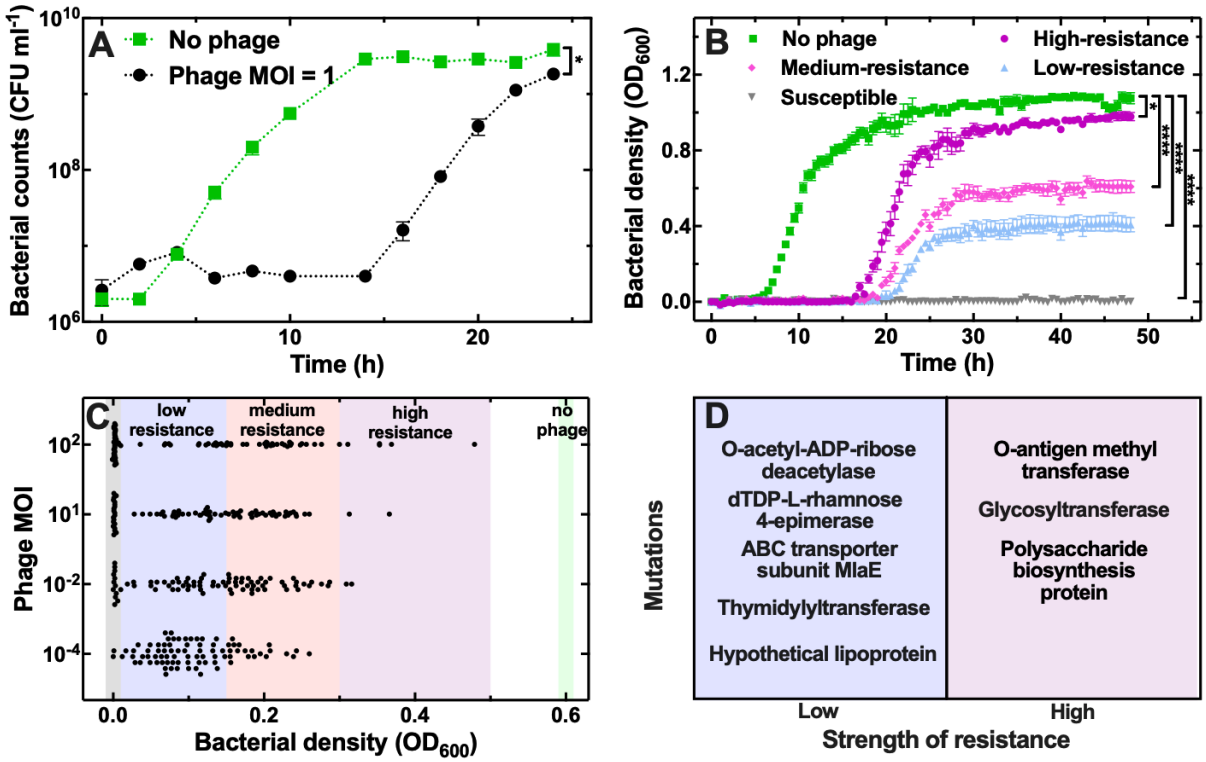

Figure 1 Heterogenous resistance to ΦBp-AMP1 in *B. thailandensis*. (A) Regrowth of stationary phase *B. thailandensis* populations in the presence of LB medium only (green squares) or together with phage at an MOI of 1 (black circles). Symbols and error bars are means and standard errors of the means of CFU measurements obtained from biological triplicates each containing technical triplicates. Very small error bars cannot be visualised due to overlap with the datapoints. Dotted lines are guides-for-the-eye. Corresponding phage counts are reported in Figure S1. (B) Regrowth of stationary phase *B. thailandensis* populations in the presence of LB medium only ($1.05 < OD_{600} < 1.2$ after 48 h, green squares) or together with phage at an MOI of 1 with different levels of bacterial resistance to phage emerging: high-resistance ($0.9 < OD_{600} < 1.05$ after 48 h, purple circles), medium-resistance ($0.5 < OD_{600} < 0.7$ after 48 h, magenta diamonds), low-resistance ($0.3 < OD_{600} < 0.5$ after 48 h, blue upward triangles), susceptible ($0 < OD_{600} < 0.01$ after 48 h, grey downward triangles). Symbols and error bars are means and standard errors of bacterial density values, measured in OD_{600}, obtained from 84 technical replicates from biological triplicates. Very small error bars cannot be visualised due to overlap with the datapoints. * indicate a p-value < 0.05, **** indicate a p-value < 0.0001. (C). Bacterial density measurements after 24 h in the presence of phage at an MOI of 10^{-4}, 10^{-2}, 1 and 10^{2}. Each black circle represents a bacterial density value performed on one of 84 technical micro-culture replicates from biological triplicates. The coloured vertical bands in the background indicate the range of OD_{600} values for each level of resistance after 24 h: high-resistance ($0.3 < OD_{600} < 0.5$, purple band), medium-resistance ($0.15 < OD_{600} < 0.3$, magenta band), low-resistance ($0.01 < OD_{600} < 0.15$, blue band), susceptibility ($0 < OD_{600} < 0.01$, grey band). (D) Unique mutations identified in five representative low- and high-resistance mutants. See Table S1 for further details.

The phage population instead increased within the first 4 h of co-incubation and reached a plateau after 6 h (Figure S1). The bacterial population started to increase after 14 h co-incubation with phage and after 24 h reached a plateau 2-fold lower compared to that

138 measured in the absence of phage (Figure 1A). These data suggest that a bacterial
139 subpopulation survives phage treatment, passes on phage immunity to its progeny and
140 becomes the predominant genotype within the population; in contrast, a susceptible
141 subpopulation becomes a minority due to phage infection but persists in the presence of phage
142 since the phage population does not decline within our experimental time frame (Figure S1).

143 To test this hypothesis, we infected 84 different stationary phase bacterial micro-cultures and
144 measured the bacterial density in the presence of phage and LB medium. We found that some
145 bacterial micro-cultures contained only bacteria that were susceptible to phage and did not
146 grow; whereas in other bacterial micro-cultures genetic resistance to phage emerged and the
147 cultures started to regrow in the presence of LB medium, albeit with different onset times,
148 slopes and saturations of growth (Figure 1B). Overall, the distribution of growth levels
149 observed could be described by a hurdle-gamma distribution (Figure 1C and Figure S2),
150 where the hurdle describes the cultures that are susceptible to phage, whereas the gamma
151 describes the spread of growth in the cultures that are resistant to phage. These data suggest
152 that *B. thailandensis* populations must contain a heterogeneous pool of mutants that are
153 resistant to the phage.

154 Next, we set out to investigate whether the phage MOI has an impact on the emergence of a
155 heterogeneous pool of genetically resistant mutants. We infected 84 stationary phase bacterial
156 micro-cultures with four different phage MOIs and measured the bacterial density after 24 h.
157 We found that the proportion of cultures susceptible to phage increased with the MOI; the
158 fraction of cultures displaying low resistance to phage or high resistance to phage reduced
159 and increased, respectively, with increasing phage MOI (Figure 1C and Figure S2). Moreover,
160 all of the cultures grew when treated with ΦBp-AMP1 at an MOI of 1 at 25 °C (Figure S3),
161 confirming that ΦBp-AMP1 features a temperature-dependent switch from the lytic to the
162 lysogenic cycle.

163 To investigate the mechanisms underpinning resistance to phage, we harvested survivor
164 populations from the experiments above and inoculated them either into 96-well plates or onto
165 agar plates containing phage. We found that all survivors grew in the presence of ΦBp-AMP1
166 and LB medium, suggesting that the bacterial populations had become genetically resistant to
167 phage. However, the colonies produced by these resistant mutants were smaller compared to
168 the parental strain (Figure S4), suggesting that these mutations brought about a fitness cost
169 [24]. Therefore, we set out to understand which genetic mutations had emerged within the
170 population during phage treatment. We sequenced the genome of five representative high-
171 resistant and low-resistant survivor cultures. We found that low resistance was due to unique
172 mutations in genes encoding the O-acetyl-ADP-ribose deacetylase, the dTDP-L-rhamnose-4-

173 epimerase, the ABC transporter subunit MlaE, the thymidylyltransferase and a hypothetical
174 lipoprotein (Figure 1D and Table S1). High resistance was instead due to unique mutations of
175 three genes encoding the O-antigen methyl transferase, a glycosyltransferase and a
176 polysaccharide biosynthesis protein. Moreover, we did not find lysogenic ΦBp-AMP1 in any
177 of the genomes sequenced (Table S2), suggesting that stable lysogeny did not occur at 37
178 °C. We found two common temperate bacteriophages of *Burkholderia* species, ΦE12-2 and
179 ΦE125, in all sequenced *B. thailandensis* genomes (Table S2).

180 Taken together, these data suggest that ΦBp-AMP1 is a lytic phage of *B. thailandensis* at 37
181 °C, that different levels of genetic resistance can emerge within putatively clonal populations
182 of *B. thailandensis* depending on the phage MOI employed and that mutations of genes
183 encoding membrane associated proteins confer high resistance to ΦBp-AMP1. Therefore, in
184 order to make ΦBp-AMP1 effective in eradicating stationary phase *B. thailandensis* there is a
185 need to use this phage in combination with clinically relevant antibiotics.

186

187 **ΦBp-AMP1 phage increases the growth inhibitory efficacy of quinolones, β-lactams and**
188 **tetracyclines**

189 We set out to investigate whether the use of ΦBp-AMP1 increases the efficacy of clinically
190 relevant antibiotics in inhibiting the regrowth of stationary phase *B. thailandensis* when
191 incubated in LB medium. We used four major antibiotic classes commonly employed for
192 treatment of melioidosis, namely quinolones, β-lactams, tetracyclines and tetrahydrofolate
193 synthesis inhibitors as well as antimicrobial agents that are not routinely employed to treat
194 melioidosis, namely aminoglycosides, oxazolidinones, macrolides and glycopeptides (Table
195 1). We determined the fractional inhibitory concentration (FIC) index of each antibiotic against
196 stationary phase *B. thailandensis* by dividing the minimum inhibitory concentration (MIC)
197 derived from combination therapy with phage at an MOI of 1 by the MIC of antibiotic
198 monotherapy. Therefore, the smaller the FIC index value measured, the higher is the increase
199 in antibiotic efficacy of the combination therapy.

200 Remarkably, combination therapy increased the efficacy of a diverse range of molecules
201 representative of all of the fluoroquinolone generations. Specifically, we measured an FIC
202 index of 0.25 for nalidixic acid (1st generation fluoroquinolone), 0.06 for ciprofloxacin (2nd
203 generation), 0.125 for levofloxacin (3rd generation), 0.125 for moxifloxacin (4th generation) and
204 0.03 for finafloxacin (5th generation). Similarly, combination therapy increased the efficacy of
205 representative β-lactams and tetracyclines against *B. thailandensis*; however, combination
206 therapy did not increase the efficacy of tetrahydrofolate synthesis inhibitors (Table 1).

Class	Molecule	Monotherapy MIC (μg ml^{-1})	Co-treatment MIC (μg ml^{-1})	FIC
Quinolones	Nalidixic Acid	16	4	0.25
	Ciprofloxacin	2	0.125	0.06
	Ofloxacin	4	0.5	0.125
	Levofloxacin	4	0.5	0.125
	Finafloxacin	2	0.06	0.03
	Moxifloxacin	2	0.25	0.125
β-Lactams	Amoxicillin	64	16	0.25
	Ampicillin	64	16	0.25
	Cefaclor	256	64	0.25
	Ceftazidime	2	0.25	0.125
	Meropenem	8	2	0.25
Tetracyclines	Doxycycline	4	1	0.25
	Tetracycline	8	2	0.25
Tetrahydrofolate Synthesis Inhibitors	Trimethoprim (TMP)	32	32	1
	Sulfamethoxazole (SMX)	1024	1024	1
	Co-trimoxazole (TMP/SMX)	32/160	32/160	1
Aminoglycosides	Gentamicin	>512	>512	-
	Streptomycin	>512	>512	-
Oxazolidinones	Linezolid	>512	>512	-
Macrolides	Roxithromycin	>512	>512	-
Glycopeptides	Vancomycin	>512	>512	-

Table 1 ΦBp-AMP1 phage increases the inhibitory efficacy of quinolones, β-lactams and tetracyclines. Antibiotic class, antibiotic molecule, minimum inhibitory concentration (MIC) measured against stationary phase *B. thailandensis* when used as monotherapy or in combination therapy with phage ΦBp-AMP1 at an MOI of 1 and the fractional inhibitory concentration (FIC) as the ratio of the MIC value obtained from the combination therapy over the MIC value obtained from monotherapy. The initial bacterial inoculum was 5×10^5 cells mL^{-1}, regrowth of stationary phase bacteria was measured as optical density after 24 h of monotherapy or combination therapy compared with regrowth of untreated stationary phase bacteria incubated in LB medium only. The MIC value after 24 h was determined as the antibiotic concentration value for which the bacterial growth was less than 10% the growth value measured for untreated bacteria. Each measurement was performed in biological triplicates each consisting of five technical replicates.

Inspired by these successful combination therapy findings, we set out to determine whether combination therapy with phage increased the efficacy of antibiotics that are not routinely

221 employed to treat melioidosis. However, combination therapy with phage did not increase the
222 efficacy of two aminoglycosides, an oxazolidinone, a macrolide or a glycopeptide (Table 1),
223 antibiotics against which *B. thailandensis* is intrinsically resistant due to constitutively
224 expressed efflux pumps and an atypical lipopolysaccharide structure [2].

225 Next, we investigated the bacterial population dynamics in the presence of phage and a sub-
226 inhibitory concentration of levofloxacin, cefaclor or trimethoprim for which combination therapy
227 with phage provided high, medium or no increase in efficacy, respectively (Table 1).
228 Combination therapy with 0.25× MIC levofloxacin and phage at an MOI of 1 in LB medium did
229 not allow for regrowth of stationary phase *B. thailandensis* within the 24 h experimental
230 timeframe, whereas regrowth started after 5 h exposure to levofloxacin monotherapy and 16
231 h after exposure to phage monotherapy (Figure 2A).

232
233
234
235

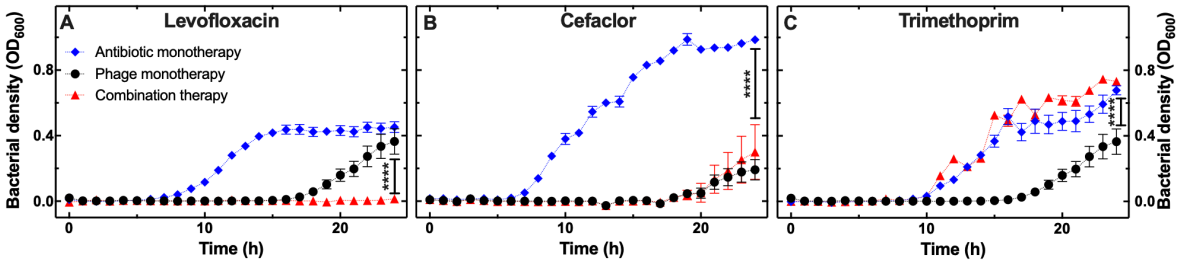

236 **Figure 2 Bacterial population dynamics in the presence of ΦBp-AMP1 and sub-inhibitory**
antibiotic concentrations. Regrowth of stationary phase *B. thailandensis* populations in the presence
237 of LB medium and either phage at an MOI of 1 (black circles), or 0.25× MIC of (A) levofloxacin, (B)
cefaclor or (C) trimethoprim either as monotherapy (blue diamonds) or in combination therapy with
238 phage at an MOI of 1 (red triangles). Symbols and error bars are means and standard errors of the
means of bacterial density values, measured in OD_{600}, obtained from biological triplicates each
consisting of five technical replicates. Very small error bars cannot be visualised due to overlap with
239 the datapoints. Dotted lines are guides-for-the-eye. **** indicate a p-value < 0.0001.

240 Following cefaclor monotherapy at 0.25× its MIC, the stationary phase *B. thailandensis*
241 population started to regrow after 5 h, whereas following either phage monotherapy at an MOI
242 of 1 or combination therapy with 0.25× MIC cefaclor and phage at an MOI of 1, the stationary
243 phase *B. thailandensis* population started to regrow after 16 h and reached a plateau that was
244 significantly lower compared to cefaclor monotherapy (Figure 2B). Following trimethoprim
245 monotherapy at 0.25× its MIC, the stationary phase *B. thailandensis* population started to
246 regrow after 9 h. Similarly, following combination therapy with 0.25× MIC trimethoprim and
247 phage at an MOI of 1, the stationary phase *B. thailandensis* population started to regrow after
248 9 h and after 24 h reached a plateau that was significantly higher compared to that reached
249 during phage monotherapy (red triangles and black circles in Figure 2C, respectively).

250 Taken together these data demonstrate that combination therapy with phage ΦBp-AMP1
251 increases the inhibitory efficacy of quinolones, β-lactams and tetracyclines, whilst combination

252 therapy with tetrahydrofolate synthesis inhibitors decreases the inhibitory efficacy of ΦBp-
253 AMP1.

254 **The interactions between phage ΦBp-AMP1 and antibiotics depend on the antibiotic**
255 **but not on the phage concentration**

256 Next, we set out to understand whether phage-antibiotic interactions in inhibiting bacterial
257 growth depend on either the antibiotic or the phage concentration. Firstly, we measured the
258 bacterial density of stationary phase *B. thailandensis* over time during exposure to LB medium
259 and different antibiotic concentrations at a constant phage MOI of 1 (data points in Figure 3A,
260 Figure 3F and Figure 3K). In order to estimate bacterial density and the associated uncertainty
261 also for antibiotic concentrations that we did not investigate experimentally, we fitted these
262 data to a statistical non-linear regression model (lines and bands in Figure 3A, Figure 3F and
263 Figure 3K). This model also allowed us to infer the probability of additivism between the phage
264 effect and the antibiotic effect on bacterial growth. We summarised our results in the form of
265 interaction plots [34] reporting bacterial density values in the absence of phage or antibiotic,
266 growth values following phage or antibiotic monotherapies and growth values following
267 combination therapy.

268 When ciprofloxacin was used above its MIC, we measured growth suppression following both
269 monotherapy and combination therapy (Figure 3A), without additive effect (blue shaded area
270 in Figure 3B and Figure 3E) in line with previous reports [34]. In contrast, when ciprofloxacin was
271 used at sub-inhibitory concentrations, the model predicted an interacting region: successful
272 growth suppression was achieved only in the case of combination therapy (red lines in Figure
273 3A), with a degree of confidence of >95% in predicted additive effect at ciprofloxacin
274 concentrations between 0.06 and 2 μg ml^{-1} (red shaded area in Figure 3B and Figure 3D).
275 This additive concentration range was broad for ciprofloxacin, finafloxacin and moxifloxacin
276 and narrower for nalidixic acid, ofloxacin and levofloxacin (Table S3). Finally, we did not record
277 an interaction effect between phage and ciprofloxacin at low concentrations (white shaded
278 area in Figure 3B and Figure 3C) in line with previous reports [34].

279 We recorded similar concentration-dependent interactions between phage and cefaclor
280 (Figure 3F-J); however, for this antibiotic the additive effect was limited to the antibiotic range
281 64-256 μg mL^{-1}, i.e. a 4-fold additive concentration range (Figure 3G). In addition, ceftazidime,
282 meropenem, doxycycline, tetracycline, amoxicillin and ampicillin displayed a narrow additive
283 concentration range (Table S3).

284

285

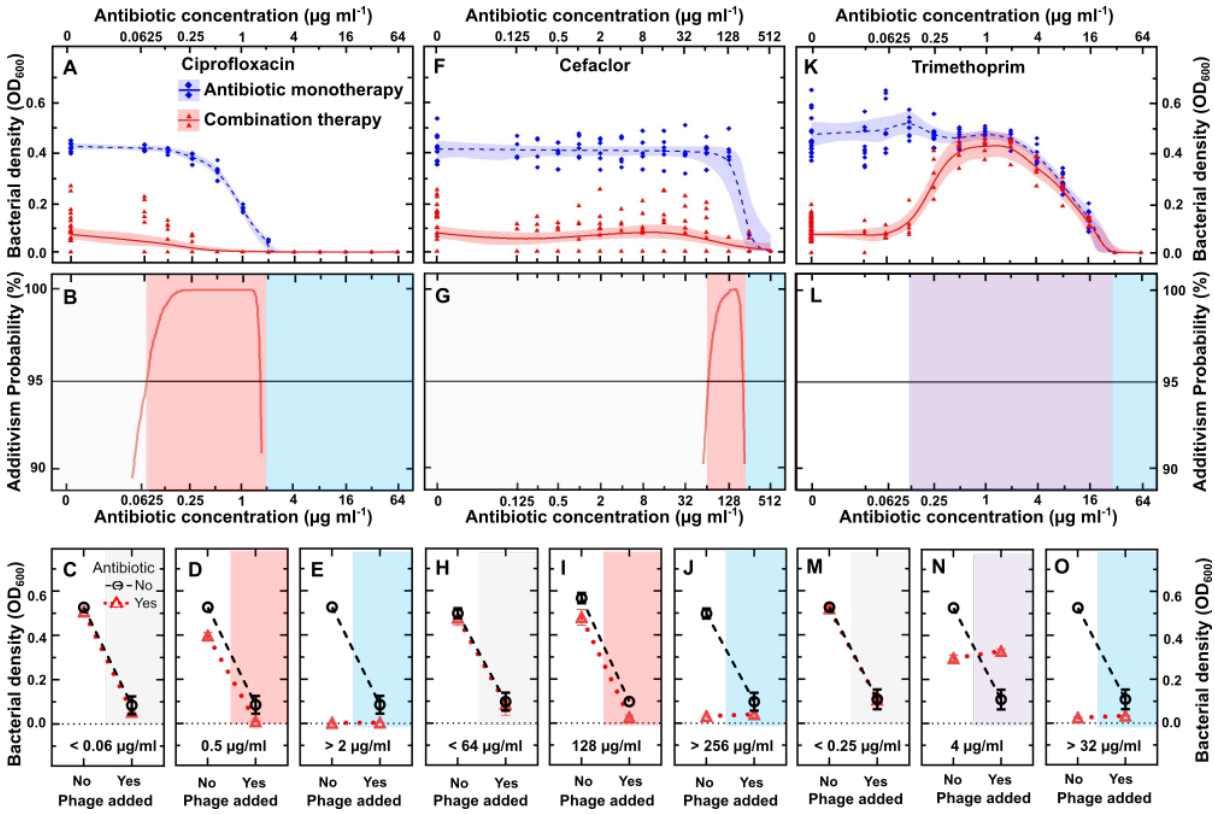

Figure 3 Interactions between ΦBp-AMP1 and antibiotics depend on the antibiotic concentration. Experimental data (symbols) and model predictions (lines and bands) describing the dependence of bacterial density on the concentration of (A) ciprofloxacin, (F) cefaclor or (K) trimethoprim in the absence (blue diamonds) and presence of phage ΦBp-AMP1 at an MOI of 1 (red triangles) after 24 h treatment. Each symbol represents the bacterial density measured in one of 15 technical replicates collated from biological triplicates. Some of the symbols overlap with each other. The lines and shaded areas are the medians, upper and lower quartiles, estimated by fitting our statistical non-linear regression model to our experimental data via Markov Chain Monte Carlo simulations. Corresponding predicted probability of an additive interaction between phage and (B) ciprofloxacin, (G) cefaclor and (L) trimethoprim (red lines) is shown only for antibiotic concentration ranges where the probability is higher than 90% (red shaded areas). Not shaded or blue shaded areas indicate antibiotic concentration ranges where the phage or the antibiotic dominate, respectively. Purple shaded areas indicate antagonism. Corresponding interaction plots at antibiotic concentrations selected from the ranges above for (C-E) ciprofloxacin, (H-J) cefaclor and (M-O) trimethoprim. Black circles connected by dashed lines show bacterial density values following control experiments and phage monotherapy, red triangles connected by dotted lines show bacterial density values following antibiotic monotherapy and combination therapy.

In contrast, we found an antagonistic effect when phage was used in combination with trimethoprim concentrations in the range of 0.125-32 µg mL^{-1} with the line connecting the growth value following antibiotic therapy and combination therapy (red, dotted line in Figure 3N) having a less negative slope than the line connecting the growth value following control experiments and phage monotherapy (black, dashed line in Figure 3N). A similarly extended antagonistic range was recorded when phage was used in combination with either sulfamethoxazole or co-trimoxazole.

Secondly, we measured the bacterial density of stationary phase *B. thailandensis* over time during incubation in LB medium while simultaneously varying the initial antibiotic concentration and phage MOI. We used ciprofloxacin, ampicillin and trimethoprim as representative molecules displaying a broad additive concentration range, a narrow additive concentration range and antagonism, respectively, in combination with phage at an initial MOI of either 10^{-4}, 10^{-2}, 10^{0} or 10^{2}. We found that growth inhibition was significantly extended below the MIC of ciprofloxacin or ampicillin even at a phage MOI of 10^{-4} (Figure 4A and Figure 4B), suggesting that a modest phage concentration is sufficient for increasing ciprofloxacin and ampicillin inhibitory efficacy against *B. thailandensis*.

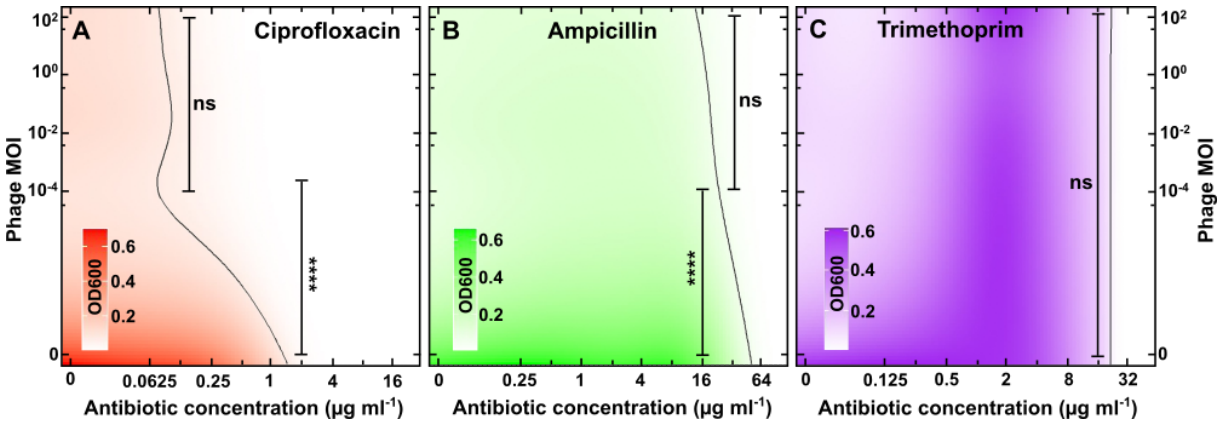

Figure 4 Phage-antibiotic interactions are not affected by the phage concentration. Heatmaps of *B. thailandensis* density (measured in OD_{600}) after 24 h treatment with different initial phage MOIs and different concentrations of (A) ciprofloxacin, (B) ampicillin or (C) trimethoprim. Heatmaps were obtained via hierarchical Bayesian statistical modelling fitted to our experimental data (measured only at the phage and antibiotic concentrations indicated on the x- and y-axes). The vertical black lines are predictions of all antibiotic-phage combinations that permit bacterial density values that are lower than 10% of the bacterial density values obtained for bacteria growing in LB medium only. ns indicates no statistical significance, **** indicates a p-value < 0.0001.

In contrast, growth inhibition was not extended below the MIC of trimethoprim at any of the phage MOIs tested (Figure 4C). Moreover, in the presence of phage *B. thailandensis* growth was maximal for trimethoprim concentrations in the range 1 - 8 μg mL^{-1} and decreased at lower trimethoprim concentrations (Figure 4C). Therefore, these data confirm the hypothesis above that sub-inhibitory concentrations of trimethoprim antagonize with phage efficacy to inhibit bacterial growth. Taken together, these data demonstrate that the interaction between phage ΦBp-AMP1 and antibiotics strongly depends on the antibiotic concentration and mode of action but not on the initial phage MOI.

Synergistic bactericidal effect of phage and ciprofloxacin in combination therapy

We next set out to quantify the bactericidal efficacy of phage-antibiotic combination therapy. We exposed stationary phase *B. thailandensis* to a range of concentrations of ciprofloxacin

344 and phage at an MOI of 1 for 24 h, we quantified bactericidal efficacy by measuring survivors
345 via CFU assays and calculated the survivor fold reduction compared to untreated bacteria (i.e.
346 the higher the fold reduction in Figure 5A the stronger the bactericidal effect). Combined with
347 phage, sub-MIC concentrations of ciprofloxacin allowed for a survivor fold reduction that was
348 between 3 and 120 times greater compared to ciprofloxacin monotherapy (red and blue bars
349 in Figure 5A, respectively, p-value < 0.0001 for all pair-wise comparisons); thus, suggesting a
350 synergistic bactericidal effect between phage and ciprofloxacin, considering that phage
351 monotherapy provided only a 2-fold survivor reduction (Figure 5A). Moreover, at supra-MIC
352 concentrations, combination therapy achieved a survivor fold reduction that was between 570
353 and 2400 times greater compared to ciprofloxacin monotherapy (p-value < 0.0001 for all pair-
354 wise comparisons a part from 8× MIC). Notably, the minimum bactericidal concentration that
355 provided complete eradication of stationary phase *B. thailandensis* (horizontal band in Figure
356 5A) was 8× MIC for ciprofloxacin monotherapy and 4× MIC for phage-ciprofloxacin

357
358
359
360
361

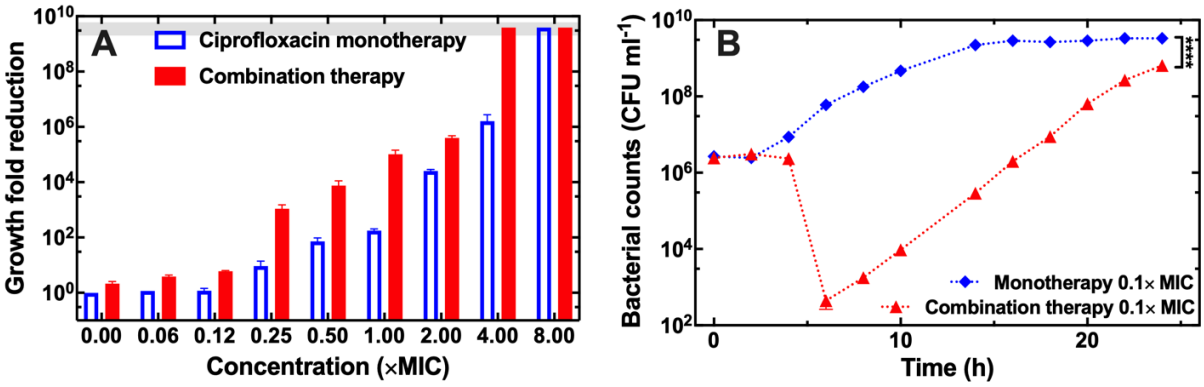

362

Figure 5 Synergistic bactericidal effect of phage and ciprofloxacin combination therapy. (A)
363 Dependence of the ratio between the number of bacteria viable after 24 h incubation in LB medium and the number of bacteria viable 24 h ciprofloxacin monotherapy (blue bars) or phage-ciprofloxacin combination therapy (red bars) on the concentration of ciprofloxacin employed. In all cases the starting
364 inoculum was stationary phase *B. thailandensis* at a concentration of 5×10^5 CFU mL^{-1} and bacteria were counted at 24 h via CFU assays. The grey horizontal band represents a survival fold reduction
365 that corresponds to the complete eradication of the bacterial population, i.e. colony counts below limit of detection of 10 CFU mL^{-1}. Pair-wise t-tests revealed that combination therapy yielded a significantly
366 (p-value < 0.0001) higher growth reduction at all ciprofloxacin concentrations tested compared to ciprofloxacin monotherapy, a part from 8× MIC. (B) Temporal dependence of bacterial counts following
367 0.125× MIC ciprofloxacin monotherapy (blue diamonds) or combination therapy with 0.125× MIC ciprofloxacin and phage at an MOI of 1 (red triangles). Symbols and error bars are means and standard errors of the mean of biological triplicates each containing technical triplicates. Very small error
368 bars cannot be visualised due to overlap with the datapoints. Dotted lines are guides-for-the-eye.

369

370 Next, we set out to measure and contrast the dynamics of the bactericidal effect of mono- and
371 combination therapy at a sub-MIC antibiotic concentration. We treated stationary phase *B.*
372 *thailandensis* with either ciprofloxacin at 0.125× its MIC or a combination of phage at an MOI
373 of 1 and ciprofloxacin at 0.125× its MIC and measured the number of survivors at regular time
374 points via CFU assays (Figure 5B). Following ciprofloxacin monotherapy, the bacterial

375 population was not affected by antibiotic exposure but started expanding after 2h of treatment
376 and reached stationary phase after 14h of treatment (blue diamonds in Figure 5B). In contrast,
377 following combination therapy the bacterial population reduced between 4 h and 6 h and
378 reached a minimum that was >5-log lower compared to the initial bacterial inoculum (red
379 triangles in Figure 5B). The surviving bacterial population started to increase after 6 h of
380 treatment due to the emergence of phage resistance (Figure S5) and reached a maximum
381 level at 24 h that was 1-log lower than bacteria treated with ciprofloxacin monotherapy (red
382 triangles and blue diamonds in Figure 5B, respectively). Taken together these data confirm
383 that the use of ΦBp-AMP1 allows a reduction in the concentration of antibiotic required to both
384 inhibit growth of or kill stationary phase *B. thailandensis*.

385

386 **Synergistic bactericidal interactions between phage and antibiotics are underpinned**
387 **by phage-induced downregulation of efflux in *B. thailandensis***

388 Next, we set out to discover the molecular mechanisms underpinning the newly found
389 synergistic bactericidal interaction between ΦBp-AMP1 and ciprofloxacin. We treated
390 stationary phase *B. thailandensis* for 4 h either with 0.125× MIC ciprofloxacin monotherapy or
391 phage monotherapy at an MOI of 1 or combination therapy with both 0.125× MIC ciprofloxacin
392 and phage at an MOI of 1. We chose 4 h-long treatments because these treatments returned
393 similar survivor numbers before the > 5-log reduction in survivor numbers measured for
394 combination therapy at the 6 h time point (Figure 5B). We extracted bacterial and phage RNA
395 from biological triplicates of each condition and performed a global comparative transcriptomic
396 analysis [39] among the transcriptomes obtained from these three different conditions and with
397 respect to stationary phase *B. thailandensis* incubated in LB medium for 4 h (Supplementary
398 files 1-3). Using principal component analysis, we found that bacterial transcriptome replicates
399 from each condition clustered together and were well separated from replicates from different
400 conditions (Figure S6A). The only exception were the bacterial transcriptomes harvested from
401 cultures treated with phage mono- and combination therapy (black circles and red triangles in
402 Figure S6A) that largely overlapped, suggesting that, at the concentrations employed, phage
403 had a greater impact than ciprofloxacin on the bacterial transcriptomes. Moreover, the phage
404 transcriptomes harvested from cultures treated with mono- and combination therapies also
405 largely overlapped according to our principal component analysis (Figure S6B).

406 Gene ontology enrichment analysis [40] of differentially expressed genes revealed that all
407 treatments investigated resulted in the downregulation of locomotion processes, in
408 accordance with a recent study using *P. aeruginosa* [41], as well as cell localization, cell
409 projection, organelle organization and response to external stimuli processes (Figure 6A, 6B

410 and Supplementary files 4-6). Ciprofloxacin monotherapy also caused the downregulation of
411 biological processes involved in cell communication, as well as the upregulation of RNA,
412 catabolic, metabolic and ribosomal processes (Figure 6A and Supplementary file 4).

413
414
415
416
417
418
419
420
421
422
423
424

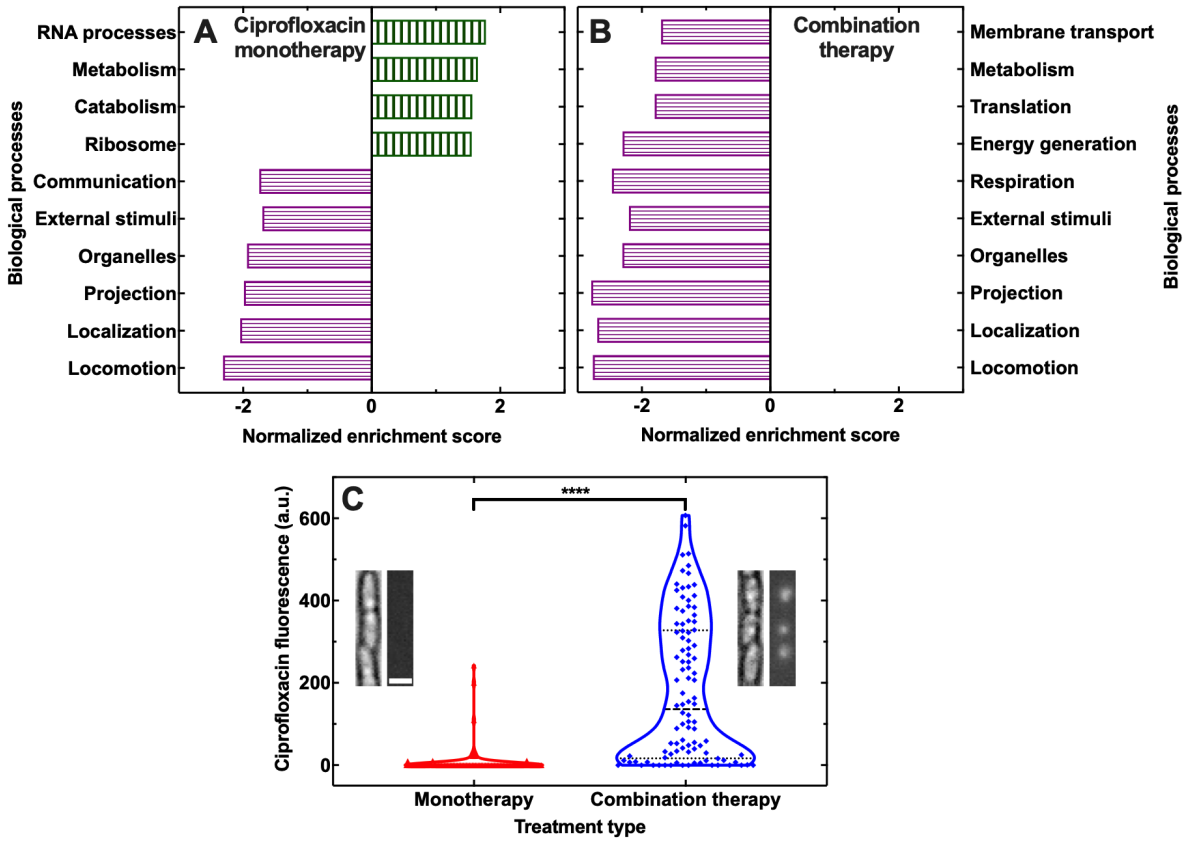

425 **Figure 6 Synergistic bactericidal interactions between phage and ciprofloxacin are underpinned by phage-induced downregulation of membrane transport in *B. thailandensis*.** Major biological
426 processes that are significantly enriched and either up- or downregulated (vertically and horizontally patterned bars, respectively) in stationary phase *B. thailandensis* after 4 h of (A) monotherapy with
427 ciprofloxacin at 0.125× MIC or (B) combination therapy with ciprofloxacin at 0.125× MIC and phage at an MOI of 1 with respect to untreated *B. thailandensis* incubated for 4 h in LB medium only.
428 Corresponding differential gene expression analyses and gene ontology enrichment analyses are reported in Supplementary files 1-3 and 4-6, respectively. (C) Distribution of values of fluorescence of ciprofloxacin-NBD accumulating in N = 100 individual stationary phase *B. thailandensis* that had been
429 incubated for 4 h in either ciprofloxacin-NBD only or ciprofloxacin-NBD and phage (red triangles and blue diamonds, respectively). Ciprofloxacin-NBD was introduced in the microfluidic device at t = 0 at a
430 concentration of 32 µg ml^{-1}, phage was introduced at t = 0 at a concentration of 10^8 PFU ml^{-1}. Dashed lines indicate the median of each distribution, dotted lines indicate the quartiles of each distribution. **** indicate a p-value < 0.0001.
431

432 In contrast, both phage monotherapy and combination therapy caused the downregulation of
433 metabolic, membrane transport, translational, energy generation and respiration processes
434 (Figure 6B and Supplementary files 5 and 6). Specifically, genes encoding the major efflux
435 pump BpeEF-OprC were significantly downregulated along with functional subunits of the
436 F_0F_1-type ATP synthases, of the cytochrome O oxidase, of the NADH-quinone oxidoreductase
437 complex, of lipopolysaccharide transport and of secretion systems (Supplementary file 2).

438 Combination therapy drove a global differential gene regulation that was very similar to that
439 caused by phage monotherapy and gene ontology enrichment analysis did not return any
440 enriched functional category for this comparison. Moreover, the expression of phage encoded
441 genes was also unaffected by the presence of ciprofloxacin (Supplementary file 7) and gene
442 ontology enrichment analysis did not return any enriched functional category for this
443 comparison either.

444 Next, we set out to test the hypothesis that phage-induced downregulation of efflux processes
445 led to increased intracellular accumulation of ciprofloxacin during phage-ciprofloxacin
446 combination therapy. We used our recently reported microfluidics-based time-lapse
447 microscopy platform [42,43] and a fluorescent derivative of ciprofloxacin (i.e. ciprofloxacin-
448 nitrobenzoxadiazole, henceforth ciprofloxacin-NBD) to measure intracellular accumulation of
449 ciprofloxacin in individual stationary phase *B. thailandensis* cells. In accordance with our
450 hypothesis, we found that the distribution of ciprofloxacin-NBD fluorescence values after 4 h
451 phage-ciprofloxacin-NBD combination therapy was significantly higher than the distribution of
452 ciprofloxacin-NBD fluorescence values after 4 h ciprofloxacin-NBD monotherapy (Figure 6C).

453 Moreover, using this platform we did not find evidence of either cell filamentation or a
454 significant difference in cell size between stationary phase *B. thailandensis* incubated in LB
455 growth medium only (Figure S7 A-E), or during phage monotherapy (Figure S7 F-J) or during
456 combination therapy with phage at an MOI of 1 and ciprofloxacin at 0.125× MIC (Figure S7 K-
457 O). We found that stationary phase *B. thailandensis* infected with phage in the presence of
458 sub-inhibitory concentrations of ampicillin or ciprofloxacin produced less phage particles than
459 in the absence of antibiotics in planktonic cultures and plaques of similar size on agar cultures
460 (Figure S1 and S8, respectively). Sub-inhibitory concentrations of trimethoprim also led to
461 smaller plaques with phage propagation starting significantly later in the presence of
462 trimethoprim (Figure S1 and S8). We also did not observe plaque formation on LB agar plates
463 in the presence of sub-inhibitory concentrations of ciprofloxacin in the absence of phage ΦBp-
464 AMP1. Moreover, in our phage transcriptome analysis we found evidence of expression of
465 structural phage proteins, but we did not find evidence of expression of genes encoding
466 excisionases, i.e. proteins required for the excision of dormant phage from within the hosts
467 genome [44], neither during phage mono- nor combination therapy (Supplementary file 7).
468 However, it is conceivable that one or more of the 11 hypothetical proteins expressed by ΦBp-
469 AMP1 (Supplementary file 7) could perform excisionase activity.

470 Taken together these data demonstrate that the observed phage-antibiotic interactions are
471 not due to cell filamentation, increase phage particle production or phage induction in the
472 presence of antibiotics but are instead underpinned by phage-induced downregulation of

473 membrane transport and energetic processes that are involved in the efflux of ciprofloxacin
474 leading to higher intracellular ciprofloxacin accumulation in the presence of phage.

475

476 **Discussion**

Emergence of resistance to phage

477 Phage and bacteria are engaged in a constant arms race leading to the evolution of a multitude
478 of non-mutually exclusive antiphage defence mechanisms, including the well-understood
479 phage receptor alteration, restriction-modification, abortive infection, CRISPR-Cas systems,
480 as well as new defence systems [45,46]. It is well established that increased phage virulence
481 selects for the evolution of host resistance if the costs associated with resistance are
482 outweighed by the benefits of the capability to avoid infection [47,48]. Accordingly, we found that
483 the level of resistance to phage increased with the strength of phage predation. Interestingly,
484 even within a putatively clonal *B. thailandensis* population we found evidence of emergence
485 of different levels of resistance due to mutations in eight different genes. Three of these genes
486 encoded glycosyltransferase and O-antigen synthesis, that are strongly linked with the LPS
487 [49], and capsular polysaccharides. Our data therefore suggest that the LPS or capsular
488 polysaccharides could be the receptors for phage ΦBp-AMP1. This hypothesis is further
489 corroborated by our global comparative transcriptomics analysis demonstrating the
490 downregulation of LPS assembly associated genes following exposure to ΦBp-AMP1. Indeed,
491 the LPS is a well-known receptor for many different bacteriophages and mutations of LPS
492 confer resistance to phage in a variety of bacteria [50–53], whereas capsular polysaccharides
493 have recently been shown to serve as primary receptors of *E. coli* phage [54,55]. Moreover, it has
494 been reported that *B. pseudomallei* displays various colony morphotypes based on O-antigen
495 variations [56]. Accordingly, we have demonstrated that phage-resistant bacteria form smaller
496 colonies compared with the parental strain while displaying mutations in genes associated
497 with O-antigen synthesis.

498 **Phage-antibiotic interactions**

499 The interactions between two or more antimicrobials as components of combination therapies
500 are broadly classified in three main types: additive (the sum of the effect of each component),
501 synergistic (a larger-than-additive effect) and antagonistic (a smaller-than-additive effect
502 [13,57,58]). In the context of phage-antibiotic therapy instead, phage-antibiotic synergy has been
503 defined as the stimulation of phage replication when bacteria are treated with sub-inhibitory
504 concentrations of antibiotics [28,29,59]. Considering that in accordance with a recent report [60] we
505 did not find stimulation of phage replication in the presence of antibiotics, we chose to use the

506 more broadly accepted definitions of additive, synergistic and antagonistic interactions,
507 introduced above [13,57,58]. Specifically, by using statistical analysis on interaction plots we found
508 an additive effect between the phage and most of the tested molecules from the quinolone, β-
509 lactam and tetracycline antibiotic classes, antagonism between the phage and
510 tetrahydrofolate synthesis inhibitors and bactericidal synergy between the phage and the
511 quinolone ciprofloxacin. These effects were comparable or more efficient in suppressing
512 bacterial growth than previously reported synergistic phage-antibiotic effects [28,33,34]. For
513 example, ceftazidime efficacy increased by a factor of 2 compared to ceftazidime monotherapy
514 when used in combination with the podovirus vB_BpP_HN01 [61] or the myovirus KS12 [9] against
515 *B. pseudomallei* or *B. cenocepacia*, respectively; we measured an 8-fold increase in
516 ceftazidime efficacy against *B. thailandensis* in the presence of phage ΦBp-AMP1. Using the
517 temperate phage HK97 in combination with ciprofloxacin, a previous study has reported
518 bactericidal synergy against *E. coli* K12, with complete eradication being achieved at 0.5× MIC
519 ciprofloxacin [32]; we measured a comparatively weaker bactericidal synergy between ΦBp-
520 AMP1 and ciprofloxacin, with complete eradication being achieved at 4× MIC ciprofloxacin.
521 However, it is worth noting that stationary phase *B. thailandensis* is significantly more resistant
522 than exponential phase *E. coli* K12 with ciprofloxacin MIC values of 2 and 0.2 μg/ml,
523 respectively.

524 **Factors affecting phage-antibiotic interactions**

525 The dependence of phage-antibiotic interactions on the antibiotic class is well established
526 [28,29,34,59,60,62], however, the mechanisms underpinning this dependence remain largely
527 unknown. For example, the myovirus KS12 broadly synergised with quinolones, β-lactams
528 and tetracycline when used to inhibit growth of *B. cenocepacia* but antagonised with
529 aminoglycosides [29]. The myovirus ΦHP3 displayed a synergistic effect with ceftazidime, an
530 additive effect with kanamycin and an antagonistic effect with chloramphenicol when used to
531 inhibit growth of *E. coli* [34]. The phage PYO^{SA} antagonised tetracycline, azithromycin, and
532 linezolid but synergised with daptomycin, vancomycin and kanamycin when used to inhibit
533 growth of *S. aureus* [33]. Here we advance this understanding by showing that even molecules
534 within the same class can display a dramatically different extent and range of additive
535 interactions with the same phage and that when used with phage the same molecule can
536 simultaneously display an additive effect in inhibiting bacterial growth and a synergistic effect
537 in killing bacteria.

538 The outcome of phage-antibiotic therapy is often contradictory because of a lack of systematic
539 analysis of interactions between phage and antibiotics: these interactions are often studied
540 with only one or two concentrations of the antimicrobials, which are wholly insufficient in

predicting combinatorial concentrations that are effective during treatment [20]. By assessing bacterial growth when exposed to multiple orders of magnitude of antibiotic concentrations and phage titers, we discovered that phage-antibiotic interactions strongly depend on the antibiotic concentration employed, but surprisingly do not vary with phage titer, a key difference from previous findings [34]. These newly discovered dependences should be taken into account when designing rational phage-antibiotic therapy [20,21]. In fact, our data suggest that it might be relatively straightforward to hit a suitable ΦBp-AMP1 phage titer in an *in vivo* setting, where phage are broadly tolerated [63] but their pharmacokinetic and pharmacodynamic parameters are less known compared to antibiotics [64].

Mechanistic understanding of phage-antibiotic interactions

The additive effects between phage and antibiotics are stronger and broader in our experiments compared to previous reports [29,59,61], possibly due to differences at the phage level, i.e., a podovirus vs a myovirus, at the bacterial strain and physiology level, i.e., stationary phase *B. thailandensis* vs exponential phase *B. cenocepacia*, or due to a different mechanism of interaction between phage and antibiotics. Indeed, KS12 and a variety of other phage displayed an increase in plaque size and phage titer in the presence of sub-inhibitory concentrations of antibiotics [26,28,31,59], possibly caused by the acceleration of phage assembly and cell lysis due to cell filamentation in the presence of antibiotics [28,29,34,65]. In contrast, we did not find evidence neither of cell filamentation nor of an increase in plaque size and phage titer in the presence of sub-inhibitory concentrations of quinolones, β-lactams or tetracyclines. Reduced phage titer in the presence of sub-inhibitory concentrations of trimethoprim could instead explain the observed antagonism between ΦBp-AMP1 and trimethoprim. Moreover, temperate phage activity is known to enhance antibiotic efficacy through depletion of lysogens [32]. Although we found evidence of prophage ΦE125 and ΦE12-2 [85,86], it is unlikely that depletion of ΦE125 or ΦE12-2 lysogens plays a role in our experiments since we did not find evidence of plaque formation in the presence of ciprofloxacin, that is a lysogen activating antibiotic [32], in the absence of ΦBp-AMP1.

Based on our global gene expression analysis, we hypothesized that antibiotics are more effective in inhibiting *B. thailandensis* growth in the presence of ΦBp-AMP1 due to phage-induced down-regulation of antibiotic efflux out of the cell. Indeed, the multi-drug efflux pump BpeEF-OprC [8] was downregulated in the presence of phage and it is known that deletion of BpeEF-OprC causes increased susceptibility to quinolones and β-lactams [9]. Moreover, we detected a strong downregulation of genes associated with aerobic respiration and transmembrane transport of protons, effectively reducing the availability of ATP for active transport of substrates as well as the proton motive force. A reduction in proton motive force

levels leads to reduced antibiotic efflux [66–68], and in the long-term selection for mutations in drug efflux components [69]. In accordance with our hypothesis, we found that a fluorescent derivative of ciprofloxacin accumulates in individual *B. thailandensis* cells at significantly higher levels in the presence of ΦBp-AMP1 compared with in its absence. Noteworthy, previous studies using phage that have the efflux component TolC as a receptor, demonstrated that emergence of phage resistance in bacteria via *tolC* mutations led to increased antibiotic susceptibility [52,70]. Finally, it is conceivable that the phage-antibiotic interactions we observed are also due to phage and antibiotics targeting cells in different metabolic states as recently hypothesised [60].

In summary, the interactions between phage and bacteria are multifaceted and complex due to a billion-year long arms race between both entities [71–75] and are further modified when a second selective pressure is imposed, such as the presence of antibiotic compounds secreted by other microbes in the environment [76]. Understanding such interactions might hold the key for successful antimicrobial therapy and to overcome the current antimicrobial resistance crisis. Considering that stationary phase bacteria are traditionally refractory to antibiotics, especially in spatial structures such as biofilms where antibiotic diffusion is further hindered [42], our data offer a potential route for their eradication by combining low doses of clinically relevant antibiotics with low doses of phage, that should be easily obtainable *in vivo* thanks to the self-propagating nature of phage.

595 **Materials and Methods:**

596 **Key Resources Table**

REAGENT or RESOURCE	Source	Identifier
Bacterial and phage strains		
B. thailandensis E264	(Kim et al., 2005)	RefSeq: NC_007650/51
ΦBp-AMP1	(Gatedee et al., 2011)	RefSeq: NC_047743
Chemicals		
Amoxicillin	Sigma-Aldrich	Cat# A8523
Ampicillin	Sigma-Aldrich	Cat# A9518
Cefaclor	Sigma-Aldrich	Cat# C6895
Ceftazidime	Melford	Cat# C59200
Ciprofloxacin	Sigma-Aldrich	Cat# 17850
Doxycycline	Sigma-Aldrich	Cat# D9891
Finafloxacin	Sigma-Aldrich	Cat# SML2134
Levofloxacin	Sigma-Aldrich	Cat# 40922
Linezolid	Sigma-Aldrich	Cat# O9409
Meropenem	Sigma-Aldrich	Cat# M2574
Moxifloxacin	Sigma-Aldrich	Cat# PHR1542
Nalidixic acid	Sigma-Aldrich	Cat# N8878
Ofloxacin	Sigma-Aldrich	Cat# O8757
Roxithromycin	Sigma-Aldrich	Cat# R4393
Sulfamethoxazole	Sigma-Aldrich	Cat# S7507
Tetracycline	Sigma-Aldrich	Cat# 87128
Trimethoprim	Sigma-Aldrich	Cat# T7883
Vancomycin	Sigma-Aldrich	Cat# 94747
Software and algorithms		
R version 3.4.1	(R Core Team, 2017)	https://cran.r-project.org
brms R package	(Bürkner, 2017)	https://cran.r-project.org
breseq	(Deathrage and Barrick,	https://barrickslab.org
ImageJ	(Schneider et al., 2012)	https://imagej.nih.gov
GraphPad Prism 8.3.0	GraphPad	https://www.graphpad.com/
PHASTER	University of Alberta, Canada	https://phaster.ca
Other		
CLARIOstar plate reader	BMG Labtech	
WPA cell density meter	Scientific Laboratory Supplies	Cat# CO8000
Sartorius Minisart™ 0.2 µm	Fisher Scientific	Cat# 10730792
RNeasy Mini Kit (50)	QIAGEN	Cat# 74104
Qubit 1.0 Fluorometer	Invitrogen	Cat# Q32857
IX73	Olympus, Tokyo, Japan	
UPLSAPO60XW	Olympus, Tokyo, Japan	
Flow Unit S	Fluigent	
MFCS-4C	Fluigent	
Zyla 4.2	Andor	

597

598

599 **Bacterial and bacteriophage strains**

600 *B. thailandensis* E264 strain and the temperature dependent, lytic bacteriophage ΦBp-AMP1
601 were obtained from the Department of Immunology, Faculty of Medicine Siriraj Hospital,
602 Mahidol University.

603 **Bacterial culturing**

604 *B. thailandensis* was stored at -80 °C and streaked on Lysogeny broth (LB, 10 g/L Tryptone,
605 5 g/L Yeast extract, 10 g/L NaCl, Melford) agar plates (10 g/L, 1.5% Agar) every two weeks.
606 Overnight cultures were setup by inoculating a single *B. thailandensis* colony from a plate into
607 flasks containing 50 mL of LB broth and were grown for 17 h at 37 °C on shaking platforms
608 set at 200 rpm.

609 **Propagation and titration of phage**

610 Phage propagation was carried out as previously reported [77]. Briefly, overnight cultures of *B.*
611 *thailandensis* E264 were diluted 1000× in 50 mL LB medium to obtain a bacterial concentration
612 of approximately 2×10^6 CFU mL^{-1}. These sub-cultures were then incubated for 4 h at 37 °C
613 and 200 rpm, allowing them to reach early exponential phase (~8×10^6 CFU mL^{-1}). Then, these
614 sub-cultures were infected with ΦBp-AMP1 at an MOI = 0.01 and incubated for 17 h at 37 °C
615 and 200 rpm. On the following day, cells were pelleted by centrifugation for 40 minutes at 3000
616 *g* and the phage-containing supernatant was filtered twice (Sartorius Minisart™ 0.2 µm) to
617 obtain a phage stock. The phage concentration within this stock was then determined via the
618 double agar overlay technique [76]. Briefly, LB top agar (10 g/L, 0.5% Agar) was melted in a
619 microwave and allowed to cool to below 40 °C. An aliquot of an overnight *B. thailandensis*
620 E264 culture was added to the melted top agar at a volume: volume concentration of 1:50. LB
621 agar plates were subsequently coated in a thin layer of the top agar above creating a
622 continuous bacterial lawn. In parallel, a 10-fold dilution series of the phage stock was prepared
623 in LB medium. Phage was then titred using the standard double agar overlay technique [103].
624 All plates were then incubated at 37 °C for 17 h after which the phage induced plaques in the
625 bacterial lawn were counted and the plaque forming units (PFU) per mL^{-1} of the phage stock
626 was calculated. Phage stocks were stored at 4 °C for a maximum of two weeks before a new
627 propagation was performed. Prior to each use, the phage concentration within the phage stock
628 was determined via the double agar overlay technique above.

629 **Bacterial growth in the presence of phage**

630 In order to measure the growth of bacteria in the presence of phage, we used two independent
631 approaches. Firstly, we measured the concentration of bacteria during phage infection over

632 time using colony forming unit (CFU) assays [78]. Briefly, three overnight cultures of *B.*
633 *thailandensis* were diluted in 50 mL LB medium to obtain a bacterial concentration of
634 approximately 2×10^6 CFU mL^{-1}. ΦBp-AMP1 was added to these three sub-cultures at an MOI
635 of 1 and the sub-cultures were incubated at 37 °C and 200 rpm. Triplicate aliquots were taken
636 from each infected sub-culture every two hours, serially diluted in LB and plated on LB agar
637 plates. These plates were incubated 37 °C for 24h before counting CFU on each plate to
638 calculate the bacterial concentration at each time point in each sub-culture as the mean and
639 standard error of the mean of biological triplicate each containing technical triplicate. The
640 growth of control uninfected cultures was measured in a similar manner without the addition
641 of phage. Secondly, we measured the change of bacterial density over time during phage
642 infection by measuring the optical density of growing sub-cultures. Briefly, three overnight
643 cultures of *B. thailandensis* were diluted in LB in the wells of a 96 well plate and mixed with
644 phage to obtain a final bacterial concentration of 5×10^5 CFU mL^{-1} and a final phage MOI of
645 either 10^{-4}, 10^{-2}, 1 or 10^2. The plates were the incubated at 37 °C and 200 rpm and the optical
646 density of each well was measured every 10 min via a CLARIOstar plate reader system (BMG)
647 and blank corrected to the optical density measured in wells containing LB medium only. Each
648 condition was tested in 84 technical replicates obtained from biological triplicate.

649 **Determination of heritable resistance to phage**

650 In order to determine whether heritable resistance to phage had emerged in bacteria from
651 wells where we measured bacterial growth in the presence of phage, we re-inoculated these
652 survivors in wells of a 96-well plate containing LB and phage at a concentration of ~5×10^5
653 PFU mL^{-1}. We incubated these plates at 37 °C and 200 rpm for 24 h and measured the optical
654 density as described above. We employed this same approach to determine whether heritable
655 resistance to phage had emerged in bacteria from wells where we measured bacterial growth
656 in the presence of both phage and each of the antibiotics reported in Table 1.

657 **Determination of colony size**

658 To determine whether phage-resistance comes at a fitness cost in colony size we performed
659 image analysis experiments of bacteria from wells where we measured bacterial growth in the
660 presence of phage. These survivors were plated onto LB agar plates alongside uninfected
661 bacteria from separate control experiments. The plates were then incubated at 37 °C for 72 h
662 and were imaged with a Xiaomi Mi A2 mobile phone camera at 24 h intervals. The colony size
663 was determined via image analysis of 150 colonies for each condition and time point using the
664 ImageJ software.

665

666 **Determination of antibiotic minimum inhibitory concentrations and the impact of phage**
667 **on antibiotic efficacy**

668 The minimum inhibitory concentration (MIC) of each antibiotic employed was determined via
669 the broth dilution method [79]. Briefly, each antibiotic was dissolved according to the
670 manufacture's specifications and diluted in a two-fold dilution series in LB medium within wells
671 of a 96-well plate. Stationary *B. thailandensis* E264 bacteria were then added at a final
672 concentration of 5×10^5 CFU mL^{-1} to each well. The plates were incubated at 37 °C and 200
673 rpm and after 24 h the optical density of each well was measured via a CLARIOstar plate
674 reader system (BMG) and blank corrected to the optical density measured in wells containing
675 LB medium only. The minimum inhibitory concentration was determined as the minimum
676 concentration of antibiotic for which we measured an optical density value that was less than
677 10% of the optical density value that we measured in wells containing LB medium and bacteria
678 only. All MIC assays were performed at least in biological and technical triplicate from which
679 mean and standard error of the mean were calculated. Next, to determine the influence of
680 ΦBp-AMP1 on the efficacy of each antibiotic, the experiments above were repeated with the
681 addition of ΦBp-AMP1 at an MOI of 1 (i.e. 5×10^5 PFU mL^{-1}).

682 **Phage growth in the presence of antibiotics**

683 Overnight cultures of *B. thailandensis* E264 were diluted 1000× in 50 mL LB medium to obtain
684 a bacterial concentration of approximately 2×10^6 CFU mL^{-1}. ΦBp-AMP1 was added to these
685 sub-cultures at an MOI of 1 and the sub-cultures were incubated at 37 °C and 200 rpm. In
686 separate experiments, ΦBp-AMP1 was added at an MOI of 1 together with either ampicillin or
687 ciprofloxacin or trimethoprim at 0.25× their respective MIC. 1 mL triplicate aliquots were taken
688 from the infected sub-cultures at two-hour intervals for twenty-four hours and the phage
689 propagation over time was monitored by determining plaque forming units per millilitre via the
690 double agar overlay technique above. Each experiment was then performed in biological
691 triplicate.

692 **Determination of time-dependent bacterial growth in the presence of antibiotic and**
693 **phage**

694 Overnight cultures of *B. thailandensis* E264 were diluted to a concentration of ~5×10^5 CFU
695 mL^{-1} in LB medium in wells of a 96-well plate, together with either ΦBp-AMP1 at an MOI of 1,
696 or levofloxacin, cefaclor or trimethoprim at 0.25× their respective MIC, or both ΦBp-AMP1 at
697 an MOI of 1 and either levofloxacin, cefaclor or trimethoprim at 0.25× their respective MIC.
698 Each plate was then incubated for 24 h in a CLARIOstar plate reader (BMG) at 37 °C and 200
699 rpm, measuring optical density at λ=600nm (OD_{600}) every 30 min. Each experiment was

700 repeated in biological and technical triplicate from which we calculated mean and standard
701 error of the mean of each measurement.

702 **Bacterial killing assays**

703 Bacterial killing assays were performed as previously reported [39]. Briefly, overnight cultures of
704 *B. thailandensis* E264 were diluted 1000× in 50 mL fresh LB growth medium and infected with
705 either solely ciprofloxacin (at a concentration between 0.625× and 8× the MIC), or a
706 combination of ciprofloxacin and phage at MOI = 1. The cultures were incubated at 37 °C and
707 200 rpm for 24 h after which the colony count (CFU mL^{-1}) was determined as reported above.
708 We quantified bactericidal efficacy of each treatment as the ratio of the colony counts in
709 untreated control experiments over the colony counts measured in each treatment.

710 **Determination of heritable resistance to antibiotics**

711 In order to determine whether heritable resistance to antibiotics had emerged in bacteria from
712 wells where we measured bacterial growth in the presence of phage and antibiotics, we re-
713 inoculated these survivors in wells of a 96-well plate containing LB and either phage at a
714 concentration of ~5×10^5 PFU mL^{-1}, or the antibiotic employed at a concentration in range
715 0.125-128 µg ml^{-1}, or both phage at a concentration of ~5×10^5 PFU mL^{-1} and the antibiotic
716 employed at a concentration in range 0.125-128 µg ml^{-1}. We incubated these plates at 37 °C
717 and 200 rpm for 24 h and measured the optical density as described above.

718 **Determination of the impact of antibiotics on plaque size**

719 To determine whether phage plaque sizes may be influenced by the presence of antibiotics,
720 we implemented a previously reported protocol [28]. Briefly, LB top agar was melted in a
721 microwave and allowed to cool below 40 °C. An aliquot of an overnight *B. thailandensis* E264
722 culture was added to the melted top agar at a volume: volume concentration of 1:50 alongside
723 phage at a concentration of 10^1 PFU mL^{-1} and either ciprofloxacin, trimethoprim or ampicillin
724 at 0.5× and 0.125× of their respective monotherapy MICs. The resulting mixture was added to
725 the top agar. The top agar was then well mixed by inversion, plated evenly onto LB agar plates
726 (10 g/L, 1.5% Agar) and incubated for 24 h at 37 °C. The plates were then imaged using a
727 Xiaomi Mi A2 mobile phone camera. The plaque size was determined via image analysis of
728 120 plaques for each condition in biological triplicate using the ImageJ software.

729 **Determination single-cell morphology and ciprofloxacin accumulation**

730 To measure the size and morphology of individual bacterial during phage-monotherapy or
731 antibiotic-phage combination therapy, we deployed the microfluidic mother machine device as
732 previously described [80]. Briefly, the device consists of a central channel that measures 25 µm

733 and 100 μm in height and width, respectively, and six thousand lateral side channels, each 1
734 μm in width and height and 25 μm in length [81]. Bacteria were prepared by pelleting an overnight
735 culture of *B. thailandensis* for 15 minutes at 3000 *g*. The resulting bacterial pellet was
736 resuspended at a previously optimised nominal OD_{600} of 50 in medium obtained by double
737 filtering the supernatant from the spun down culture using 0.22 μm filters [82,83]. These bacteria
738 were then introduced in the central channel of the mother machine device from where they
739 reached the lateral channel at an average concentration of one bacterium per channel [84]. Next,
740 the device was mounted on an inverted microscope (IX73 Olympus, Tokyo, Japan) located in
741 a temperature-controlled chamber kept at 37 °C [85]. Fluorinated ethylene propylene tubing
742 (1/32" × 0.008") was connected to the device as inlet and outlet tubes further connected to a
743 computerised pressure-based flow control system (MFCS-4C, Fluigent) [86]. Next, LB medium
744 only or LB medium containing 2×10^8 PFU mL^{-1} phage or LB medium containing 2×10^8 PFU
745 mL^{-1} phage and 0.125× MIC ciprofloxacin was continuously supplied in the device at a
746 constant flow rate of 100 μl/h. Simultaneously, bright field images of 20 areas of the mother
747 machine, each containing 23 lateral channels were acquired at 2 min intervals via a 60× 1.2
748 N.A. objective (UPLSAPO60XW, Olympus) and an sCMOS camera with an exposure time of
749 0.01 s (Zyla 4.2, Andor, Belfast, United Kingdom) controlled via Labview [87]. This microfluidics-
750 microscopy platform was also used to quantify the accumulation of ciprofloxacin as previously
751 reported [88,89]. Briefly, LB medium containing a fluorescent ciprofloxacin derivative, i.e.
752 ciprofloxacin-nitrobenzoxadiazole (ciprofloxacin-NBD) or ciprofloxacin-NDB and 2×10^8 PFU
753 mL^{-1} phage was continuously supplied in the device at a constant flow rate of 100 μl/h. In both
754 cases ciprofloxacin-NBD was supplied at a concentration of 32 μg ml^{-1}. Bright field images
755 were acquired as described above together with corresponding fluorescence images acquired
756 by exposing the bacteria for 0.03 s to the blue excitation band of a broad-spectrum LED
757 (CoolLED pE300white, power = 8 mW at the sample plane, Andover, UK) via a FITC filter. All
758 images were analysed using the ImageJ software as previously described [90].

759 **Determination of mutations underpinning resistance to phage**

760 In order to determine the mutations underpinning resistance to phage in bacteria from wells
761 where we measured bacterial growth in the presence of phage, we plated these survivors on
762 LB agar plates, incubated these plates at 37 °C for 24h and shipped the plates to MicrobesNG.
763 MicrobesNG performed DNA isolation and ull genome sequencing using 2×250 bp paired end
764 sequencing with a minimum coverage of 30× on the Illumina HiSeq sequencer. Analysis of the
765 sequenced genomes was performed using the *breseq* pipeline [91].

766

767

768 **Comparative bacterial and phage transcriptomic analysis**

769 RNA isolation, library preparation, sequencing, and transcriptomic data processing was
770 performed as previously reported [92]. Briefly, RNA isolation was performed using the RNeasy
771 Mini kit (QIAGEN), according to the manufacturer's specifications. Bacteria were grown in
772 triplicate for 4h in flasks containing 50 mL LB, or LB containing phage at an MOI of 1, or LB
773 containing ciprofloxacin at 0.125× MIC, or LB containing both phage at an MOI of 1 and
774 ciprofloxacin at 0.125× MIC. DNA removal during extraction was carried out using RNase-
775 Free DNase I (Qiagen). RNA concentration and quality were measured using Qubit 1.0
776 fluorometer (ThermoFisher Scientific) and 2200 TapeStation (Agilent), respectively, and only
777 samples with an RNA integrity number above 8 were sequenced using Illumina NovaSeq 6000.
778 Transcript abundance was quantified using Salmon for each gene in all samples. Subsequent
779 differential analysis was performed using DEseq2 in R software to quantify the log2 fold
780 change in transcript reads for each gene and compared across the four different experimental
781 conditions. Significantly differentially expressed genes were defined as having a log2 fold
782 change greater than 1 and a p-value adjusted for false discovery rate of < 0.05. Gene Set
783 Enrichment Analysis was performed using the clusterProfiler package for R [93]. Enrichments in
784 terms belonging to the "Biological process", "Molecular function" or "Cellular component"
785 ontology were calculated by ranking the genes by differential expression and calculating an
786 Enrichment Score (a weighted Kolmogorov–Smirnov-like statistic) for each ontology term. P
787 values were adjusted for false discovery by using the method of Benjamini and Hochberg [94].
788 Finally, the lists of significantly enriched terms were simplified to remove redundant terms, as
789 assessed via their semantic similarity to other enriched terms, using clusterProfiler's simplify
790 function.

791 **Statistical non-linear regression model**

792 We developed a statistical non-linear regression model to fit the experimental data in order to
793 estimate treatment output and the associated uncertainty also for treatment conditions that we
794 did not investigate experimentally. Since the distribution of bacterial growth values (in terms
795 of OD_{600}) in the presence of phage was skewed, we fitted our data with a Gamma distribution
796 function. Moreover, to account for inaccuracies in optical density measurements via a plate
797 reader, we assumed any measurement below an optical density of 0.05 to be equal to 'zero'.
798 Hence, the data had a non-trivial number of zero values, which could not be captured by a
799 conventional gamma distribution. To accommodate this, we included a parameter which
800 controls the probability of an experiment returning an optical density equal to zero. This two-
801 part distribution strategy resulted in what is often called a "hurdle model" [95]. This distribution
802 then had three parameters, one that represented the probability of measuring a value of zero,

and two representing the gamma distribution, in our case parameterised to have a mean parameter and a shape parameter. We assumed that these three parameters could change with the antibiotic concentration and with the phage concentration. We also assumed these relationships to be potentially non-linear. In other words, we assumed the probability of observing a value of zero, the average non-zero observation, and the spread of non-zero observations all depended on the antibiotic and phage concentrations in a complex manner. As such, we modelled these parameters using cubic regression tensor product smoothing splines [96]. Additionally, the spline knot locations for the two gamma distribution parameters were constrained to only the points where a non-zero observation was made. To fit this model, and estimate the various parameters, including splines, we used Markov Chain Monte Carlo (MCMC), using the brms R package [97], with default options used for the priors. This provided us with posterior distributions for all the unknown parameters, allowing us to make probabilistic statements and provide full uncertainty estimates. To better capture the uneven measurement intervals of empirical data and because we were interested in the relationships between antibiotic and phage concentrations, it was convenient to apply a log2 transform to the antibiotic concentration and a log10 transformation to the phage concentration values. To avoid numerical issues when the antibiotic or phage concentrations were equal to 0, we added a small value to each zero before applying the transformation (0.01 for the antibiotic data, and $1e^{-10}$ for the phage measurement data). The model allowed us to continuously predict bacterial growth in terms of optical density and the associated uncertainty for both treatment concentrations that were experimentally investigated as well as treatment concentrations that were not experimentally investigated.

Data availability

All data generated or analysed during this study are included in this published article and its supplementary information files.

Acknowledgments

This work was supported by the BBSRC through a grant awarded to S.P., K.T.A. and U.L. (BB/V008021/1). S.K. was supported by a QUEX PhD studentship awarded to S.P., M.A.T.B. and K.T.A. KTA and E.B. gratefully acknowledge the financial support of the EPSRC (EP/T017856/1). K.C., K.B. and S.H. were supported by the Defence Science and Technology Laboratory. This project utilised equipment funded by a Wellcome Trust Institutional Strategic Support Fund (WT097835MF), a Wellcome Trust Multi-User Equipment Award (WT101650MA) and a BBSRC LoLa award (BB/K003240/1). The funders had no role in study design, data collection and analysis, decision to publish, or preparation of the manuscript.

Author contributions

Conceptualization, S.P.; methodology, S.K., U.L., E.B. and E.L.A.; formal analysis, S.K., U. L., E.B. and S.P; generation of figures, S.K., U.L., E.B. and S.P; investigation, S.K., U.L., K.C., E.B., E.L.A., P.O.N., A.F., A.A. E.G., S.K., K.B., S.V.H., K.T.A., M.A.T.B. and S.P.; resources, K.T.A., M.A.T.B. and S.P.; data curation, S.K. and S.P., writing – original draft, S.K. and S.P.; writing – review & editing, S.K., U.L., K.C., E.B., E.L.A., P.O.N., A.F., A.A., E.G., S.K., K.B., S.V.H., K.T.A., M.A.T.B. and S.P.; visualization, S.K., U.L. and S.P.; supervision, S.P., M.A.T.B. and K.T.A.; project administration, S.P.; funding acquisition, S.P., M.A.T.B. and K.T.A..

Declaration of interests

We do not have any competing interests.

850 **References**

851 1. Murray, C.J., Ikuta, K.S., Sharara, F., Swetschinski, L., Robles Aguilar, G., Gray, A.,
852 Han, C., Bisignano, C., Rao, P., Wool, E., et al. (2022). Global burden of bacterial
853 antimicrobial resistance in 2019: a systematic analysis. Lancet *399*, 629–655.
854 10.1016/S0140-6736(21)02724-0.

855 2. Rhodes, K.A., and Schweizer, H.P. (2016). Antibiotic resistance in Burkholderia
856 species. Drug Resist. Updat. *28*, 82–90. 10.1016/j.drup.2016.07.003.

857 3. Mahenthiralingam, E., Urban, T.A., and Goldberg, J.B. (2005). The multifarious,
858 multireplicon Burkholderia cepacia complex. Nat. Rev. Microbiol. *3*, 144–156.
859 10.1038/nrmicro1085.

860 4. Galyov, E.E., Brett, P.J., and Deshazer, D. (2010). Molecular insights into
861 Burkholderia pseudomallei and Burkholderia mallei pathogenesis. Annu. Rev.
862 Microbiol. *64*, 495–517. 10.1146/annurev.micro.112408.134030.

863 5. Wiersinga, W.J., Virk, H.S., Torres, A.G., Currie, B.J., Peacock, S.J., Dance, D.A.B.,
864 and Limmathurotsakul, D. (2018). Melioidosis. Nat. Rev. Dis. Prim. *4*.
865 10.1038/nrdp.2017.107.

866 6. Podnecky, N.L., Rhodes, K.A., and Schweizer, H.P. (2015). Efflux pump-mediated
867 drug resistance in burkholderia. Front. Microbiol. *6*, 1–25. 10.3389/fmicb.2015.00305.

868 7. Podnecky, N.L., Wuthiekanun, V., Peacock, S.J., and Schweizer, H.P. (2013). The
869 BpeEF-OprC efflux pump is responsible for widespread trimethoprim resistance in
870 clinical and environmental Burkholderia pseudomallei isolates. Antimicrob. Agents
871 Chemother. *57*, 4381–4386. 10.1128/AAC.00660-13.

872 8. Rhodes, K.A., Somprasong, N., Podnecky, N.L., Mima, T., Chirakul, S., and
873 Schweizer, H.P. (2018). Molecular determinants of Burkholderia pseudomallei BpeEF-
874 OprC efflux pump expression. Microbiol. (United Kingdom) *164*, 1156–1167.
875 10.1099/mic.0.000691.

876 9. Krishnamoorthy, G., Weeks, J.W., Zhang, Z., Chandler, C.E., Xue, H., Schweizer,
877 H.P., Ernst, R.K., and Zgurskaya, H.I. (2019). Efflux Pumps of Burkholderia
878 thailandensis Control the Permeability Barrier of the Outer Membrane. Antimicrob.
879 Agents Chemother. *63*, 1–13. 10.1128/AAC.00956-19.

880 10. Ventola, C. (2015). The antibiotic resistance crisis: part 1: causes and threats. Pharm.
881 Ther. *40*, 277–283. 10.1016/B978-1-4831-9711-1.50022-3.

882 11. Vidal-Cortés, P., Martin-Loeches, I., Rodríguez, A., Bou, G., Cantón, R., Diaz, E., De
883 la Fuente, C., Torre-Cisneros, J., Nuvials, F.X., Salavert, M., et al. (2022). Current
884 Positioning against Severe Infections Due to Klebsiella pneumoniae in Hospitalized
885 Adults. Antibiotics *11*. 10.3390/antibiotics11091160.

886 12. Yang, Y., Guo, Y., Yin, D., Zheng, Y., Wu, S., Zhu, D., and Hu, F. (2021). In Vitro
887 Activity of Cefepime-Zidebactam, Ceftazidime- Avibactam, and Other Comparators
888 against Clinical Isolates of Enterobacterales, Pseudomonas aeruginosa, and
889 Acinetobacter baumannii: Results from China Antimicrobial Surveillance Network
890 (CHINET) in 2. Antimicrob. Agents Chemother. *65*, e01726-20. 10.1128/AAC.01726-
891 20.

892 13. Brochado, A.R., Telzerow, A., Bobonis, J., Banzhaf, M., Mateus, A., Selkrig, J., Huth,
893 E., Bassler, S., Zamarreño Beas, J., Zietek, M., et al. (2018). Species-specific activity
894 of antibacterial drug combinations. Nature *559*, 259–263. 10.1038/s41586-018-0278-
895 9.

896 14. Cacace, E., Kim, V., Varik, V., Knopp, M., Tietgen, M., Brauer-nikonow, A., Inecik, K.,
897 Mateus, A., Milanese, A., Mårli, M.T., et al. (2023). Systematic analysis of drug
898 combinations against Gram-positive bacteria. Nat. Microbiol. 10.1038/s41564-023-
899 01486-9.

900 15. Cavaco, M., Castanho, M.A.R.B., and Neves, V. (2022). The Use of Antibody-
901 Antibiotic Conjugates to Fight Bacterial Infections. Front. Microbiol. *13*.
902 10.3389/fmicb.2022.835677.

903 16. Kepiro, I.E., Marzuoli, I., Hammond, K., Ba, X., Lewis, H., Shaw, M., Gunnoo, S.B.,
904 De Santis, E., Łapińska, U., Pagliara, S., et al. (2020). Engineering Chirally Blind
905 Protein Pseudocapsids into Antibacterial Persisters. ACS Nano *14*, 1609.
906 10.1021/acsnano.9b06814.

907 17. Mayorga-Ramos, A., Zúñiga-Miranda, J., Carrera-Pacheco, S.E., Barba-Ostria, C.,
908 and Guamán, L.P. (2023). CRISPR-Cas-Based Antimicrobials: Design, Challenges,
909 and Bacterial Mechanisms of Resistance. ACS Infect. Dis. *9*, 1283–1302.
910 10.1021/acsinfecdis.2c00649.

911 18. Benítez-Chao, D.F., León-Buitimea, A., Lerma-Escalera, J.A., and Morones-Ramírez,
912 J.R. (2021). Bacteriocins: An Overview of Antimicrobial, Toxicity, and Biosafety
913 Assessment by in vivo Models. Front. Microbiol. *12*, 1–18.
914 10.3389/fmicb.2021.630695.

915 19. van Heuvel, L., Caini, S., Dückers, M.L.A., and Paget, J. (2022). Assessment of the
916 inclusion of vaccination as an intervention to reduce antimicrobial resistance in AMR
917 national action plans: a global review. Global. Health *18*, 1–10. 10.1186/s12992-022-
918 00878-6.

919 20. Strathdee, S.A., Hatfull, G.F., Mutalik, V.K., and Schooley, R.T. (2023). Phage
920 therapy: From biological mechanisms to future directions. Cell *186*, 17–31.
921 10.1016/j.cell.2022.11.017.

922 21. Kortright, K.E., Chan, B.K., Koff, J.L., and Turner, P.E. (2019). Phage Therapy: A
923 Renewed Approach to Combat Antibiotic-Resistant Bacteria. Cell Host Microbe *25*,
924 219–232. 10.1016/j.chom.2019.01.014.

925 22. Tagliaferri, T.L., Jansen, M., and Horz, H.P. (2019). Fighting Pathogenic Bacteria on
926 Two Fronts: Phages and Antibiotics as Combined Strategy. Front. Cell. Infect.
927 Microbiol. *9*, 1–13. 10.3389/fcimb.2019.00022.

928 23. Martin, I., Morales, S., Alton, E.W.F.W., and Davies, J.C. (2023). Lytic Bacteriophage
929 Is a Promising Adjunct to Common Antibiotics across Cystic Fibrosis Clinical Strains
930 and Culture Models of Pseudomonas aeruginosa Infection. Antibiotics *12*.
931 10.3390/antibiotics12030593.

932 24. Van Nieuwenhuyse, B., Van der Linden, D., Chatzis, O., Lood, C., Wagemans, J.,
933 Lavigne, R., Schroven, K., Paeshuyse, J., de Magnée, C., Sokal, E., et al. (2022).
934 Bacteriophage-antibiotic combination therapy against extensively drug-resistant
935 Pseudomonas aeruginosa infection to allow liver transplantation in a toddler. Nat.
936 Commun. *13*, 1–12. 10.1038/s41467-022-33294-w.

937 25. Jones, J.D., Trippett, C., Suleman, M., Clokie, M.R.J., and Clark, J.R. (2023). The
938 Future of Clinical Phage Therapy in the United Kingdom. Viruses *15*, 721.
939 10.3390/v15030721.

940 26. Krueger, A.P., Smith, P.N., and Mcguire, C.D. (1948). Observations on the effect of
941 penicillin on the reaction between phage and Staphylococci. J. Gen. Physiol. *31*, 477–
942 488. 10.1085/jgp.31.6.477.

943 27. Price, W.H. (1947). Bacteriophage Formation Without Bacterial Growth. J. Gen.
944 Physiol. *31*, 135–139. 10.1085/jgp.31.2.135.

945 28. Comeau, A.M., Tétart, F., Trojet, S.N., Prère, M.F., and Krisch, H.M. (2007). Phage-
946 antibiotic synergy (PAS): β-lactam and quinolone antibiotics stimulate virulent phage
947 growth. PLoS One *2*, 8–11. 10.1371/journal.pone.0000799.

948 29. Kamal, F., and Dennis, J.J. (2015). Burkholderia cepacia complex phage-antibiotic
949 synergy (PAS): Antibiotics stimulate lytic phage activity. Appl. Environ. Microbiol. *81*,
950 1132–1138. 10.1128/AEM.02850-14.

951 30. Knezevic, P., Curcin, S., Aleksic, V., Petrusic, M., and Vlaski, L. (2013). Phage-
952 antibiotic synergism: A possible approach to combatting Pseudomonas aeruginosa.
953 Res. Microbiol. *164*, 55–60. 10.1016/j.resmic.2012.08.008.

954 31. Kaur, S., Harjai, K., and Chhibber, S. (2012). Methicillin-resistant Staphylococcus
955 aureus phage plaque size enhancement using sublethal concentrations of antibiotics.
956 Appl. Environ. Microbiol. *78*, 8227–8233. 10.1128/AEM.02371-12.

957 32. Al-Anany, A.M., Fatima, R., and Hynes, A.P. (2021). Temperate phage-antibiotic
958 synergy eradicates bacteria through depletion of lysogens. Cell Rep. *35*, 109172.
959 10.1016/j.celrep.2021.109172.

960 33. Berryhill, B.A., Huseby, D.L., McCall, I.C., Hughes, D., and Levin, B.R. (2021).
961 Evaluating the potential efficacy and limitations of a phage for joint antibiotic and
962 phage therapy of Staphylococcus aureus infections. Proc. Natl. Acad. Sci. U. S. A.
963 *118*, 1–8. 10.1073/pnas.2008007118.

964 34. Liu, C.G., Green, S.I., Min, L., Clark, J.R., Salazar, K.C., Terwilliger, A.L., Kaplan,
965 H.B., Trautner, B.W., Ramig, R.F., and Maresso, A.W. (2020). Phage-antibiotic
966 synergy is driven by a unique combination of antibacterial mechanism of action and
967 stoichiometry. MBio *11*, 1–19. 10.1128/mBio.01462-20.

968 35. Shan, J., Korbsrisate, S., Withatanung, P., Adler, N.L., Clokie, M.R.J., and Galyov,
969 E.E. (2014). Temperature dependent bacteriophages of a tropical bacterial pathogen.
970 Front. Microbiol. *5*, 1–7. 10.3389/fmicb.2014.00599.

971 36. Gatedee, J., Kritsiriwuthinan, K., Galyov, E.E., Shan, J., Dubinina, E., Intarak, N.,
972 Clokie, M.R., and Korbsrisate, S. (2011). Isolation and characterization of a novel
973 podovirus which infects burkholderia pseudomallei. Virol. J. *8*, 2–6. 10.1186/1743-
974 422X-8-366.

975 37. Egilmez, H.I., Morozov, A.Y., Clokie, M.R.J., Shan, J., Letarov, A., and Galyov, E.E.
976 (2018). Temperature-dependent virus lifecycle choices may reveal and predict facets
977 of the biology of opportunistic pathogenic bacteria. Sci. Rep. *8*, 1–13.
978 10.1038/s41598-018-27716-3.

979 38. Lim, Y.M., Vadivelu, J., Mariappan, V., Venkatraman, G., and Vellasamy, K.M. (2023).
980 Effective Therapeutic Options for Melioidosis: Antibiotics versus Phage Therapy.

Pathogens *12*, 1–22. 10.3390/pathogens12010011.

39. Smith, A., Kaczmar, A., Bamford, R.A., Smith, C., Frustaci, S., Kovacs-Simon, A., O'Neill, P., Moore, K., Paszkiewicz, K., Titball, R.W., et al. (2018). The culture environment influences both gene regulation and phenotypic heterogeneity in Escherichia coli. Front. Microbiol. *9*, 1739. 10.3389/fmicb.2018.01739.

40. Glover, G., Voliotis, M., Łapińska, U., Invergo, B.M., Soanes, D., O'Neill, P., Moore, K., Nikolic, N., Petrov, P.G., Milner, D.S., et al. (2022). Nutrient and salt depletion synergistically boosts glucose metabolism in individual Escherichia coli cells. Commun. Biol. *5*, 385.

41. Brandão, A.C., Putzeys, L., Pires, D.P., Voet, M., Paeshuyse, J., Azeredo, J., and Lavigne, R. (2023). Impact of phage predation on P. aeruginosa adhered to human airway epithelium: major transcriptomic changes in metabolism and virulence-associated genes. RNA Biol. *20*, 235–247. 10.1080/15476286.2023.2216065.

42. Łapińska, U., Voliotis, M., Lee, K.K., Campey, A., Stone, M.R.L., Phetsang, W., Zhang, B., Tsaneva-Atanasova, K., Blaskovich, M.A.T., and Pagliara, S. (2022). Fast bacterial growth reduces antibiotic accumulation and efficacy. Elife *11*, e74062.

43. Attrill, E.L., Claydon, R., Łapińska, U., Recker, M., Meaden, S., Brown, A.T., Westra, E.R., Harding, S. V., and Pagliara, S. (2021). Individual bacteria in structured environments rely on phenotypic resistance to phage. PLOS Biol. *19*, e3001406. 10.1371/journal.pbio.3001406.

44. Cutts, E.E., Barry Egan, J., Dodd, I.B., and Shearwin, K.E. (2020). A quantitative binding model for the Apl protein, the dual purpose recombination-directionality factor and lysis-lysogeny regulator of bacteriophage 186. Nucleic Acids Res. *48*, 8914–8926. 10.1093/nar/gkaa655.

45. Doron, S., Melamed, S., Ofir, G., Leavitt, A., Lopatina, A., Keren, M., Amitai, G., and Sorek, R. (2018). Systematic discovery of antiphage defense systems in the microbial pangenome. Science (80-.). *359*, 0–12. 10.1126/science.aar4120.

46. Georjon, H., and Bernheim, A. (2023). The highly diverse antiphage defence systems of bacteria. Nat. Rev. Microbiol. *21*, 686–700. 10.1038/s41579-023-00934-x.

47. van Houte, S., Buckling, A., and Westra, E.R. (2016). Evolutionary Ecology of Prokaryotic Immune Mechanisms. Microbiol. Mol. Biol. Rev. *80*, 745–763. 10.1128/mmbr.00011-16.

1013 48. Wendling, C.C., Lange, J., Liesegang, H., Sieber, M., Pöhlein, A., Bunk, B., Rajkov,
1014 J., Goehlich, H., Roth, O., and Brockhurst, M.A. (2022). Higher phage virulence
1015 accelerates the evolution of host resistance. Proc. R. Soc. B Biol. Sci. *289*.
1016 10.1098/rspb.2022.1070.

1017 49. Cote, J.M., and Taylor, E.A. (2017). The glycosyltransferases of LPS core: A review of
1018 four heptosyltransferase enzymes in context. Int. J. Mol. Sci. *18*.
1019 10.3390/ijms18112256.

1020 50. Mutalik, V.K., Adler, B.A., Rishi, H.S., Piya, D., Zhong, C., Koskella, B., Kutter, E.M.,
1021 Calendar, R., Novichkov, P.S., Price, M.N., et al. (2020). High-throughput mapping of
1022 the phage resistance landscape in E. coli. PLoS Biol. *18*, e3000877.
1023 10.1371/journal.pbio.3000877.

1024 51. Warring, S.L., Malone, L.M., Jayaraman, J., Easingwood, R.A., Rigano, L.A.,
1025 Frampton, R.A., Visnovsky, S.B., Addison, S.M., Hernandez, L., Pitman, A.R., et al.
1026 (2022). A lipopolysaccharide-dependent phage infects a pseudomonad
1027 phytopathogen and can evolve to evade phage resistance. Environ. Microbiol. *24*,
1028 4834–4852. 10.1111/1462-2920.16106.

1029 52. Burmeister, A.R., Fortier, A., Roush, C., Lessing, A.J., Bender, R.G., Barahman, R.,
1030 Grant, R., Chan, B.K., and Turner, P.E. (2020). Pleiotropy complicates a trade-off
1031 between phage resistance and antibiotic resistance. Proc. Natl. Acad. Sci. U. S. A.
1032 *117*. 10.1073/pnas.1919888117.

1033 53. Wright, R.C.T., Friman, V.P., Smith, M.C.M., and Brockhurst, M.A. (2019). Resistance
1034 evolution against phage combinations depends on the timing and order of exposure.
1035 MBio *10*. 10.1128/mBio.01652-19.

1036 54. Gong, Q., Wang, X., Huang, H., Sun, Y., Qian, X., Xue, F., Ren, J., Dai, J., and Tang,
1037 F. (2021). Novel Host Recognition Mechanism of the K1 Capsule-Specific Phage of
1038 Escherichia coli : Capsular Polysaccharide as the First Receptor and
1039 Lipopolysaccharide as the Secondary Receptor . J. Virol. *95*. 10.1128/jvi.00920-21.

1040 55. Scholl, D., Adhya, S., and Merril, C. (2005). Escherichia coli K1's capsule is a barrier
1041 to bacteriophage T7. Appl. Environ. Microbiol. *71*, 4872–4874.
1042 10.1128/AEM.71.8.4872-4874.2005.

1043 56. Wikraiphat, C., Saiprom, N., Tandhavanant, S., Heiss, C., Azadi, P., Wongsuvan, G.,
1044 Tuanyok, A., Holden, M.T.G., Burtnick, M.N., Brett, P.J., et al. (2015). Colony
1045 morphology variation of Burkholderia pseudomallei is associated with antigenic

1046 variation and O-polysaccharide modification. Infect. Immun. *83*, 2127–2138.
1047 10.1128/IAI.02785-14.

1048 57. Roemhild, R., Bollenbach, T., and Andersson, D.I. (2022). The physiology and
1049 genetics of bacterial responses to antibiotic combinations. Nat. Rev. Microbiol. *20*,
1050 478–490. 10.1038/s41579-022-00700-5.

1051 58. Chait, R., Craney, A., and Kishony, R. (2007). Antibiotic interactions that select
1052 against resistance. Nature *446*, 668–671. 10.1038/nature05685.

1053 59. Mankovich, A.G., Maciel, K., Kavanaugh, M., Kistler, E., Muckle, E., and Weingart,
1054 C.L. (2023). Phage-antibiotic synergy reduces Burkholderia cenocepacia population.
1055 BMC Microbiol. *23*, 1–12. 10.1186/s12866-022-02738-0.

1056 60. Nicholls, P., Clark, J.R., Gu Liu, C., Terwilliger, A., and Maresso, A.W. (2023). Class-
1057 Driven Synergy and Antagonism between a Pseudomonas Phage and Antibiotics.
1058 Infect. Immun. *91*, e0006523. 10.1128/iai.00065-23.

1059 61. Wang, Y., Li, X., Dance, D.A.B., Xia, H., Chen, C., Luo, N., Li, A., Li, Y., Zhu, Q., Sun,
1060 Q., et al. (2022). A novel lytic phage potentially effective for phage therapy against
1061 Burkholderia pseudomallei in the tropics. Infect. Dis. Poverty *11*, 1–13.
1062 10.1186/s40249-022-01012-9.

1063 62. Tsunemoto, H., Sugie, J., Enustun, E., Pogliano, K., and Pogliano, J. (2023). Bacterial
1064 cytological profiling reveals interactions between jumbo phage ϕKZ infection and cell
1065 wall active antibiotics in Pseudomonas aeruginosa. PLoS One *18*, 1–18.
1066 10.1371/journal.pone.0280070.

1067 63. Liu, D., Van Belleghem, J.D., de Vries, C.R., Burgener, E., Chen, Q., Manasherob, R.,
1068 Aronson, J.R., Amanatullah, D.F., Tamma, P.D., and Suh, G.A. (2021). The safety
1069 and toxicity of phage therapy: A review of animal and clinical studies. Viruses *13*, 1–
1070 20. 10.3390/v13071268.

1071 64. Dąbrowska, K., and Abedon, S.T. (2019). Pharmacologically Aware Phage Therapy:
1072 Pharmacodynamic and Pharmacokinetic Obstacles to Phage Antibacterial Action in
1073 Animal and Human Bodies. Microbiol. Mol. Biol. Rev. *83*. 10.1128/mmbr.00012-19.

1074 65. Bulssico, J., Papukashvill, I., Espinosa, L., Gandon, S., and Ansaldi, M. (2023).
1075 Phage-antibiotic synergy: Cell filamentation is a key driver of successful phage
1076 predation. PLOS Pathog. *19*, e1011602. 10.1371/journal.ppat.1011602.

1077 66. Paulsen, I.T., Brown, M.H., and Skurray, R.A. (1996). Proton-dependent multidrug

1078 efflux systems. Microbiol. Rev. *60*, 575–608. 10.1128/mr.60.4.575-608.1996.

1079 67. Le, D., Krasnopeeva, E., Sinjab, F., Pilizota, T., and Kim, M. (2021). Active efflux
1080 leads to heterogeneous dissipation of proton motive force by protonophores in
1081 bacteria. MBio *12*, e00676-21. 10.1128/mBio.00676-21.

1082 68. Anes, J., McCusker, M.P., Fanning, S., and Martins, M. (2015). The ins and outs of
1083 RND efflux pumps in Escherichia coli. Front. Microbiol. *6*, 1–14.
1084 10.3389/fmicb.2015.00587.

1085 69. Griffith, J.M., Basting, P.J., Bischof, K.M., Wrona, E.P., Kunka, K.S., Tancredi, A.C.,
1086 Moore, J.P., Hyman, M.R.L., and Slonczewski, J.L. (2018). Experimental evolution of
1087 Escherichia coli K-12 in the presence of proton motive force (PMF) uncoupler
1088 carbonyl cyanide m-chlorophenylhydrazone selects for mutations affecting PMF-
1089 driven drug efflux pumps. Appl. Environ. Microbiol. *85*, 1–18. 10.1128/AEM.02792-18.

1090 70. Tamer, Y.T., Gaszek, I., Rodrigues, M., Coskun, F.S., Farid, M., Koh, A.Y., Russ, W.,
1091 and Toprak, E. (2021). The Antibiotic Efflux Protein TolC Is a Highly Evolvable Target
1092 under Colicin E1 or TLS Phage Selection. Mol. Biol. Evol. *38*, 4493–4504.
1093 10.1093/molbev/msab190.

1094 71. Hampton, H.G., Watson, B.N.J., and Fineran, P.C. (2020). The arms race between
1095 bacteria and their phage foes. Nature *577*, 327–336. 10.1038/s41586-019-1894-8.

1096 72. Chevallereau, A., Pons, B.J., van Houte, S., and Westra, E.R. (2022). Interactions
1097 between bacterial and phage communities in natural environments. Nat. Rev.
1098 Microbiol. *20*, 49–62. 10.1038/s41579-021-00602-y.

1099 73. Bohannan, B.J.M., and Lenski, R.E. (2000). Linking genetic change to community
1100 evolution: Insights from studies of bacteria and bacteriophage. Ecol. Lett. *3*, 362–377.
1101 10.1046/j.1461-0248.2000.00161.x.

1102 74. Koskella, B., and Brockhurst, M.A. (2014). Bacteria-phage coevolution as a driver of
1103 ecological and evolutionary processes in microbial communities. FEMS Microbiol.
1104 Rev. *38*, 916–931. 10.1111/1574-6976.12072.

1105 75. Koonin, E. V., Senkevich, T.G., and Dolja, V. V. (2006). The ancient virus world and
1106 evolution of cells. Biol. Direct *1*, 1–27. 10.1186/1745-6150-1-29.

1107 76. Dimitriu, T., Kurilovich, E., Łapińska, U., Severinov, K., Pagliara, S., Szczelkun, M.D.,
1108 and Westra, E.R. (2021). Bacteriostatic antibiotics promote CRISPR-Cas adaptive
1109 immunity by enabling increased spacer acquisition. Cell Host Microbe *30*, 31–40.

10.1016/j.chom.2021.11.014.

77. Attrill, E.L., Łapińska, U., Westra, E.R., Harding, S. V., and Pagliara, S. (2023). Slow growing bacteria survive bacteriophage in isolation. ISME Commun. *3*, 1–9. 10.1038/s43705-023-00299-5.

78. Goode, O., Smith, A., Łapińska, U., Attrill, E., Carr, A., Metz, J., and Pagliara, S. (2021). Heterologous Protein Expression Favors the Formation of Protein Aggregates in Persister and Viable but Nonculturable Bacteria´. ACS Infect. Dis. *7*, 1848. 10.1021/acsinfecdis.1c00154.

79. Zhang, Y., Kepiro, I., Ryadnov, M.G., and Pagliara, S. (2023). Single Cell Killing Kinetics Differentiate Phenotypic Bacterial Responses to Different Antibacterial Classes. Microbiol. Spectr. *11*, e03667-22. 10.1128/spectrum.03667-22.

80. Cama, J., and Pagliara, S. (2021). Microfluidic Single-Cell Phenotyping of the Activity of Peptide-Based Antimicrobials. In Polypeptide Materials: Methods and Protocols. Methods in Molecular Biology, pp. 237–253. 10.2307/j.ctt1ffjgqc.20.

81. Cama, J., Nahas, K. Al, Fletcher, M., Hammond, K., Ryadnov, M.G., Keyser, U.F., and Pagliara, S. (2022). An ultrasensitive microfluidic approach reveals correlations between the physico-chemical and biological activity of experimental peptide antibiotics. Sci. Rep. *12*, 4005. 10.1038/s41598-022-07973-z.

82. Cama, J., Voliotis, M., Metz, J., Smith, A., Iannucci, J., Keyser, U.F., Tsaneva-Atanasova, K., and Pagliara, S. (2020). Single-cell microfluidics facilitates the rapid quantification of antibiotic accumulation in Gram-negative bacteria. Lab Chip *20*, 2765–2775. 10.1039/d0lc00242a.

83. Lapinska, U., Glover, G., Capilla-lasheras, P., Young, A.J., and Pagliara, S. (2019). Bacterial ageing in the absence of external stressors. Philos. Trans. R. Soc. B Biol. Sci. *374*, 20180442.

84. Bamford, R.A., Smith, A., Metz, J., Glover, G., Titball, R.W., and Pagliara, S. (2017). Investigating the physiology of viable but non-culturable bacteria by microfluidics and time-lapse microscopy. BMC Biol. *15*, 121. 10.1186/s12915-017-0465-4.

85. Łapińska, U., Glover, G., Kahveci, Z., Irwin, N.A.T., Milner, D.S., Tourte, M., Albers, S.V., Santoro, A.E., Richards, T.A., and Pagliara, S. (2023). Systematic comparison of unilamellar vesicles reveals that archaeal core lipid membranes are more permeable than bacterial membranes. PLoS Biol. *21*, 1–29. 10.1371/journal.pbio.3002048.

1143 86. Pagliara, S., Chimerel, C., Langford, R., Aarts, D.G.A.L., and Keyser, U.F. (2011).
1144 Parallel sub-micrometre channels with different dimensions for laser scattering
1145 detection. Lab Chip *11*. 10.1039/c1lc20399a.

1146 87. Dettmer, S.L., Keyser, U.F., and Pagliara, S. (2014). Local characterization of
1147 hindered Brownian motion by using digital video microscopy and 3D particle tracking.
1148 Rev. Sci. Instrum. *85*. 10.1063/1.4865552.

1149 88. Blaskovich, M.A., Phetsang, W., Stone, M.R., Lapinska, U., Pagliara, S., Bhalla, R.,
1150 and Cooper, M.A. (2019). Antibiotic-derived molecular probes for bacterial imaging. In
1151 Photonic Diagnosis and Treatment of Infections and Inflammatory Diseases II, p. 2.
1152 10.1117/12.2507329.

1153 89. Stone, M.R.L., Masi, M., Phetsang, W., Pages, J.-M., Cooper, M.A., and Blaskovich,
1154 M.A.T. (2019). Fluoroquinolone-derived fluorescent probes for studies of bacterial
1155 penetration and efflux. Medchemcomm *10*, 901. 10.1039/c9md00124g.

1156 90. Smith, A., Metz, J., and Pagliara, S. (2019). MMHelper : An automated framework for
1157 the analysis of microscopy images acquired with the mother machine. Sci. Rep. *9*,
1158 10123. 10.1038/s41598-019-46567-0.

1159 91. Deatherage, D.E., and Barrick, J.E. (2014). Identification of mutations in laboratory-
1160 evolved microbes from next-generation sequencing data using breseq. Methods Mol.
1161 Biol. *1151*, 165–188. 10.1007/978-1-4939-0554-6_12.

1162 92. Goode, O., Smith, A., Zarkan, A., Cama, J., Invergo, B.M., Belgami, D., Metz, J.,
1163 Jeffries, A., Norville, I.H., David, J., et al. (2021). Persister Escherichia coli Cells Have
1164 a Lower Intracellular pH than Susceptible Cells but Maintain Their pH in Response to
1165 Antibiotic Treatment. MBio *12*, e00909-21.

1166 93. Subramanian, A., Tamayo, P., Mootha, V.K., Mukherjee, S., Ebert, B.L., Gillette, M.A.,
1167 Paulovich, A., Pomeroy, S.L., Golub, T.R., Lander, E.S., et al. (2005). Gene set
1168 enrichment analysis: A knowledge-based approach for interpreting genome-wide
1169 expression profiles. Proc. Natl. Acad. Sci. U. S. A. *102*, 15545–15550.
1170 10.1073/pnas.0506580102.

1171 94. Benjamini, Y., and Hochberg, Y. (1995). Controlling the False Discovery Rate: A
1172 Practical and Powerful Approach to Multiple Testing. J. R. Stat. Soc. B *57*, 289–300.

1173 95. Hu, M.C., Pavlicova, M., and Nunes, E. V. (2011). Zero-inflated and hurdle models of
1174 count data with extra zeros: Examples from an HIV-risk reduction intervention trial.
1175 Am. J. Drug Alcohol Abuse *37*, 367–375. 10.3109/00952990.2011.597280.

96. Wood, S.N. (2017). P-splines with derivative based penalties and tensor product smoothing of unevenly distributed data. Stat. Comput. *27*, 985–989. 10.1007/s11222-016-9666-x.

97. Bürkner, P.C. (2017). brms: An R package for Bayesian multilevel models using Stan. J. Stat. Softw. *80*. 10.18637/jss.v080.i01.